Glacier evolution in the South West slope of Nevado Hualcán

(Cordillera Blanca, Perú)

Claudia Giráldez Míner

Master Project

Master en Tecnologías de la Información Geográfica (TIG)

Universidad Complutense de Madrid

Directors:

Prof. David Palacios (UCM) and Prof. Wilfried Haeberli (University of Zurich)

Departamento de Análisis Geográfico Regional y Geografía Física

Grupo de Investigación en Geografía Física de Alta Montaña (GFAM)

TABLE OF CONTENTS

CHAPTER 1

INTRODUCTION

Glaciers are key indicators of climate change. They are also the water supply upon which depend an increasing population and a cause of natural hazards. Many Peruvians live directly beneath melting glaciers and unstable glacial lakes experiencing firsthand the consequences of global warming and glacier retreat. The aim of this work was to reconstruct earlier glacial phases in the SW slope of Nevado Hualcán in order to achieve quantitative information on surface areas and ELAs as a first step for further analysis on glacier evolution, glacier-climate relations, glacier hazards and climate change.

1.1 Geographical setting

As part of the South American Andes, the Cordillera Blanca stretches over about 180 km long by 30 km wide, between latitudes 8°30′-10°10′ S and longitudes 77º00'–78º00' W. It is located in the Peruvian State of Ancash, 400km north of the capital city of Lima. It holds 27 peaks that reach elevations of over 6.000 m, and more than 200 peaks exceed 5.000 m (Solomina et al., 2007). These high altitudes allow glaciers to exist today and to have been far more extensive in the past (Smith et al., 2008). To the west of the Cordillera Blanca is the Cordillera Negra mountain range—and between these two ranges lays the Santa River Valley, known in Peru as the Callejón de Huaylas (Carey et al., manuscript in preparation). The runoff from the Cordillera Blanca supplies the intensely cultivated Callejon de Huaylas, to be then deviated for power production in the Cañón del Pato hydropower plant. Thereafter, it flows through the extremely dry lower valley of Rio Santa and reaches the Pacific coast near Chimbote were its waters are again used for agriculture and industry (Kaser, 2003). Approximately 267.000 people inhabit the Callejón de Huaylas, with a much larger population in proximity of the Cordillera Blanca on the eastern slopes and in the lowland Santa River valley (Carey et al., manuscript in preparation). Nevado Hualcán (6.122 m) lies on the Pacific slope of Cordillera Blanca and it is separated from Nevado Huascarán by the Quebrada Ulta to its North-West.

With 722 glaciers covering a total area of 723 km² (inventoried in 1970), Cordillera Blanca is the most extensive tropical mountain range and comprises about 25% of all tropical glaciers (Kaser et al., 1990, 2003). Tropical glaciers occur in Irian Jaya (Indonesian New Guinea), on the East African Mt. Kenya, Kibo (Mt. Kilimanjaro), and Rwenzori, and in the South American Andes between Venezuela and Bolivia (Tropical Andes) (Kaser, 1999). Their total area is estimated at about 2,5x10³ km² corresponding to 4,6% of the mountain glaciers and to 0,16% of the total ice cover of the world. More than 70% of this is found in Peruvian Andes and 25% in Cordillera Blanca (Kaser, 1995).

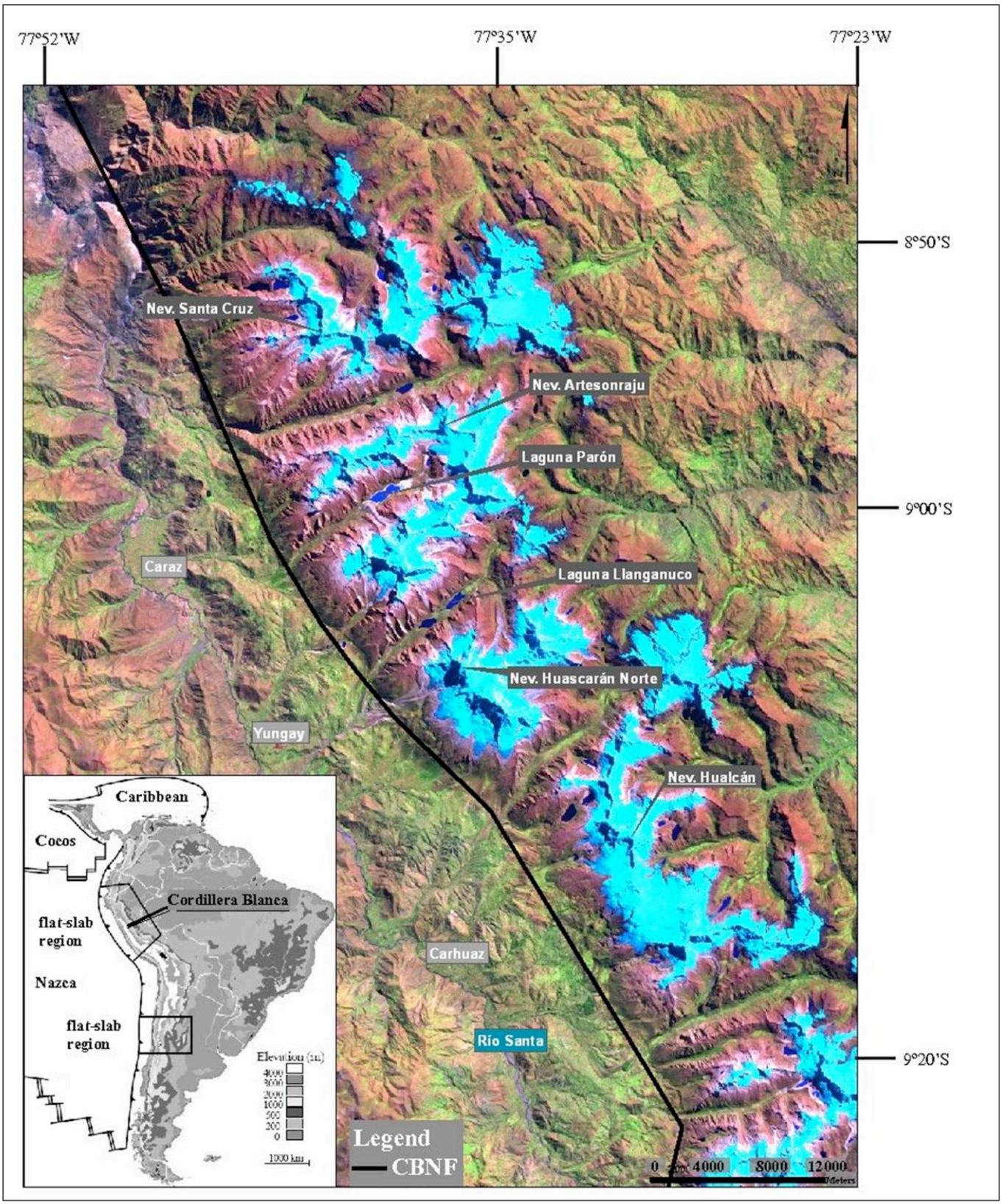

Figure 1. 1: Geographical setting of Cordillera Blanca. Bottom figure: modified from Gregory-Wodzicki (2000); Main figure: Landsat5TM, band combination 5-4-2, date 31st May 1987, from GLCF U. Maryland

From a glaciological point of view, Kaser (1995) specifies three delimitations for tropical glaciers (Fig. 1.2). They must be confined within: 1) the astronomical tropics (radiative delimitation); 2) the area where the daily temperature variation exceeds the annual temperature variation (thermal delimitation); 3) the oscillation area of the Inter Tropical Convergence Zone ITCZ (hygric delimitation). The ITCZ is the latitudinal a band where the southwesterly northern hemisphere trade winds converge with the northwesterly southern hemisphere trade winds causing a solid band of convective clouds carrying storms and intense rainfalls. Within these three boundaries, outer tropical conditions may be distinguished from the inner tropical conditions by their precipitation regime (Kaser et al., 1999). The former, to which Cordillera Blanca belongs, shows defined wet and dry seasons whereas the latter shows a rather continuous precipitation regime.

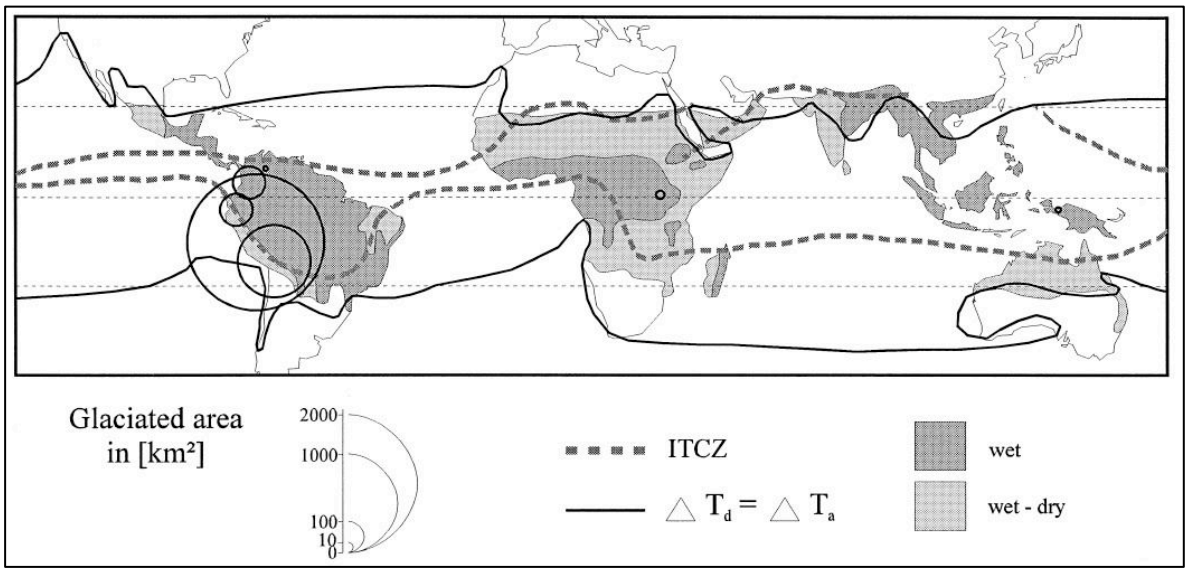

Figure 1. 2: Delimitations of tropical glaciers from a glaciological point of view, taken directly from Kaser (1999). ITCZ: Inter Tropical Convergence Zone; ΔT_d: Daily temperature variation; ΔT_a: Annual temperature variation.

In a cross-section, the Tropical Andes consist of five topographic sections (from west to east): 1) the Western Slope; 2) the Western Cordillera; 3) the high-elevation Central Andean Plateau; 4) the Eastern Cordillera (i.e Cordillera Blanca); and 5) the Subandean Zone. The Central Andean Plateau is an internally drained region with a relatively constant altitude (3.500–4.000 m) which lies between the Western and Eastern Cordillera from about lat. 11º S to 27º S. In its widest part (up to 500 km between lat. 15º and 25º S) it is known as the Altiplano in Peru and Bolivia and the Puna in Argentina (Smith et al., 2008).

1.2 Geological setting

The Andes mountain chain has developed as oceanic lithosphere of Nazca Plate underlying the eastern Pacific Ocean has been subducted beneath continental lithosphere

of the South American Plate (Smith et al., 2008). Between lat. 2º–15°S (including Cordillera Blanca) and 28°–33°30'S, the Nazca plate subducts at an angle of 5°–10° beneath the South American plate. These regions are termed "flat-slab zones" and are distinguished by a lack of late Miocene to Holocene volcanic activity (Fig. 1.1). Elsewhere along the margin, the Nazca plate subducts at an angle of 30°. These steeply dipping zones correspond to areas of young volcanism. The zone to the south of lat. 33°30'S is termed the Southern Volcanic Zone. Between 15°S and 28°S it is called the Central Volcanic Zone; and that laying north of 2°S, the Northern Volcanic Zone (Gregory-Wodzicki, 2000). It is likely that much of the final surface uplift of the Andes in northern Peru was attained in the last 5-6 Ma BP (Garver et al., 2005). Along the west margin of the mountain range, the 20º-45º west-dipping Cordillera Blanca Normal Fault (CBNF) extends for ~210 km along the range (Garver et al., 2005). McNulty (2002) recognized CBNF as the first active detachment fault to be documented above a modern flat slab.

1.3 Climatic setting

As mentioned above, Cordillera Blanca climate is typical for the outer tropics. It is characterized by relatively small seasonal but large daily temperature variations, and by the alternation of a pronounced dry season (May-September) and a wet season (October-April). The wet season brings 70- 80% of the annual precipitation (Kaser et al., 1997). Mass accumulation takes place only during the wet season and predominantly in the upper parts of the glaciers, whereas ablation occurs throughout the year reaching a maximum during the accumulation season. Thus, the vertical budget gradient is much stronger on tropical tongues than on those in the mid-latitudes (Kaser et al., 1997). Whereas Alpine glaciers show a symmetry between highest and lowest points, those of the Cordillera Blanca (e.g. Huascarán-Chopicalqui massif) do not. Here, the different altitudes of glacier origins have almost no effect on the altitudes of the tongues and they end more or less at the same elevation (Kaser, 1995). The following features of atmospheric circulation in the tropics affect the seasonal and topographical distribution of precipitation and thus the glacial regime in the Cordillera Blanca: 1) the oscillation of the cloud and precipitation belt of the ITCZ causes the seasonal distribution of precipitation in a wet and a dry season; 2) humid air is almost exclusively advected from the east, so convective activity decreases to the west and, consequently, the accumulation also decreases from east to west; 3) a superposed diurnal convective circulation system, where convective clouds are better developed in the afternoon (over the western slopes), causes a zonal asymmetry in the radiation balance and, therefore, the ablation decreases from west to east (Fig. 1.3). Decreasing convective activity to the west (2) explains that glaciers on the eastern slopes extend to generally lower elevations than those on the western slopes, and diurnal convective circulation (3) underlies the inverse asymmetry. The Cordillera Blanca is, in any case, a significant barrier in the easterly-southeasterly atmospheric circulation of humid air from the Amazon River basin causing a marked difference in annual precipitation between eastern and western slopes. Annual precipitation on the western slopes of the Cordillera

Blanca at 5.000 m is estimated to be approximately 1.200 mm, while the highest values on the eastern slopes reach approximately 3.000 mm.

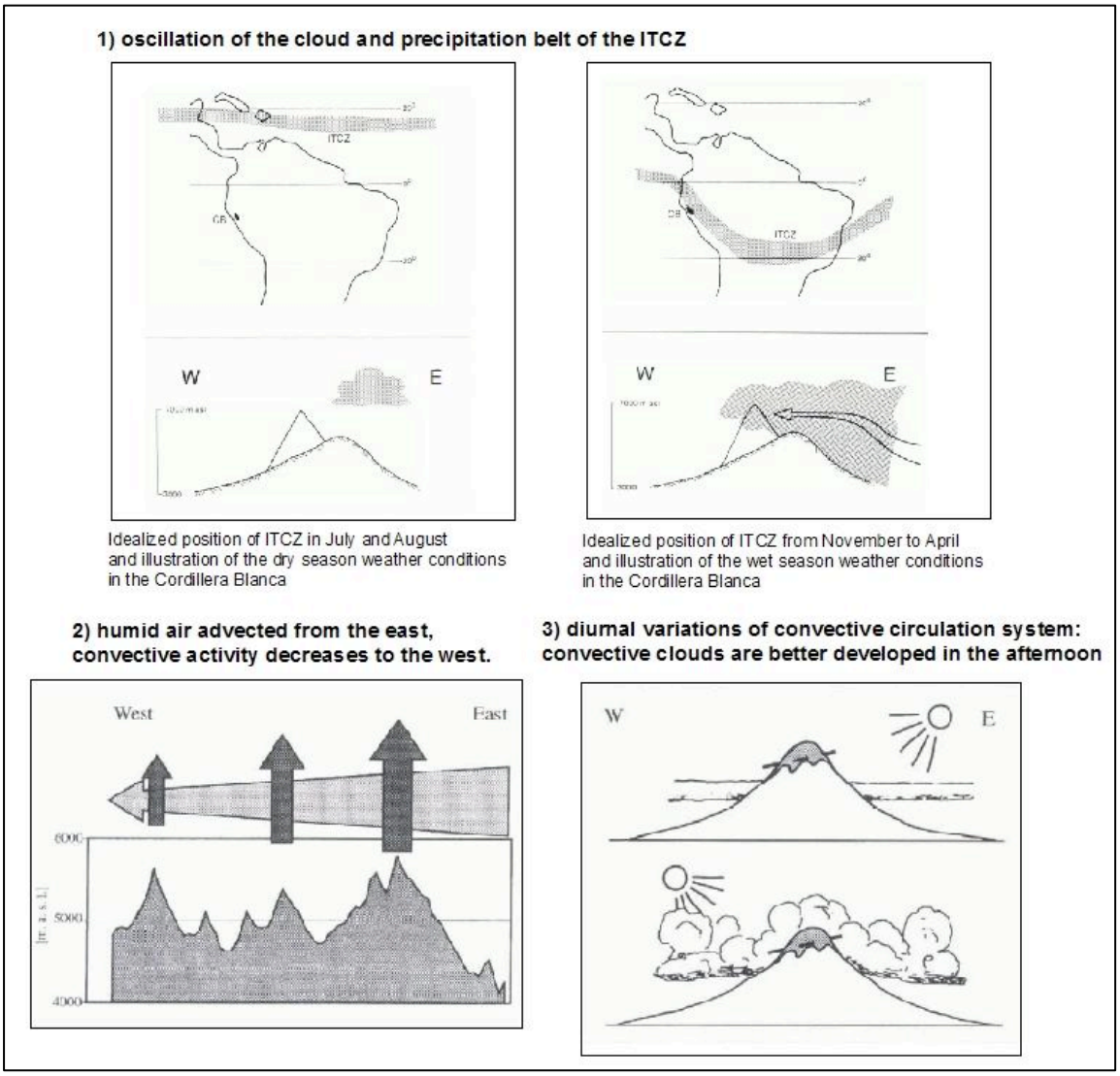

Figure 1. 3: Particularities of atmospheric circulation in the tropics, taken directly from Kaser et al. (1990) and Kaser (1997).

In 1993 Thompson drilled two ice cores on the col between the North and the South peaks of Nevado Huascarán. The paleoclimatic and environmental records derived from these cores allowed him to suggests that: 1) Late Glacial Stage (LGS) conditions at high elevations in the tropics were as much as 8º to 12º cooler than today and include evidence of the Younger Dryas (YD) cool phase; 2) Holocene began 10 ka BP, it reached its warmest conditions between 8,4 and 5,2 ka BP, and gradually cooled over the latter half of the Holocene to culminate in the Little Ice Age (LIA) cool phase; and 3) a strong warming has dominated the last two centuries (Thompson et al., 1995). The LGS ice is characterized by a contemporaneous increase in dust concentration and a decrease in ^{18}O. The end of LGS is marked by an increase in ^{18}O and reduced dust deposition which

started about 15 ka BP. The same patterns are found in the polar ice cores of Greenland (Dye 3) and Antartica (DomeC). This supports Thompson´s interpretation that Huascarán basal ice was deposited at about 19 ka BP contemporaneously with the two polar ices, and that the tropics were extremely sensitive to the cold LGS conditions. Holocene conditions are inferred from ^{18}O, NO3- and pollen records.

1.4 Glacier evolution

A significant portion of the world´s population depends upon water released seasonally from mountain glaciers and snow (Carey, 2010). In Cordillera Blanca, glacier meltwater is of crucial importance as it is the main source of fresh water during the dry season for a numerous and increasing population whose water supply for drinking and irrigation would be threatened by glacier retreat. Glacier meltwater is also important for hydropower generation which is 80% of total electricity produced in Perú (WGMS 2008, Kaser and Georges, 2003).

There have been several studies in different Peruvian regions focused on understanding glacier chronology and glacier retreat, ultimately aiming at analyzing the processes of climate change. A summary of some of these works is presented here and classified into four glacial phases: Local Last Glacial Maximum (LLGM), Younger Dryas (YD), Little Ice Age (LIA), and modern glacier fluctuations. There are several absolute dating methods that have been used for dating, but their study exceeds the purpose of this project, and will be just mentioned below.

LLGM: Farber et al. (2005) report the results of direct dating of the LGM and older moraines in four Cordillera Blanca Quebradas (Rurec, Cojup, Llaca and Queshque) using cosmogenic radionuclide dating method (CRN ^{10}Be). They suggest that glaciers emanating from the western Cordillera Blanca advanced to their maximum position by 29 ka BP at the latest, and persisted at this position until retreat initiated 20,5 ka BP. Smith et al. (2005) also reported an absolute chronology of the LLGM based on cosmogenic dating (^{10}Be) of erratics on moraines in the Junin region, 200km South-East of Cordillera Blanca. Both sets of results are consistent as they date the maximum glacial extent from 34 ka to 21 ka years BP; recession taking over by 21-20,5 ka BP followed by a still/readvance between 20 ka and 16 ka BP, and a final steady retreat after 15 ka BP. Both authors also find older moraines suggesting that the LLGM glacial advances in these regions were relatively minor compared to older advances. Farber et al. (2005) found moraines ranging from 120 ka to 440 ka BP with concentration ages around 125 ka, 225 ka and 440 ka BP, which roughly correlate with Marine Isotope Stages (MIS) 6, 8 and 12. Smith et al. (2005) found moraines in the Junin valleys that were dated about 65 ka BP and in many cases beyond 200 ka BP. Smith et al. (2005) suggest that the maximum extent of glaciation during the LGM was earlier in the tropical Andes than in the Northern Hemisphere, whereas Farber et al. (2005) review the results obtained by Balco et al. (2002) and suggested that the southeastern and southern margin of the Laurentide ice sheet reached and retreated from its maximum extent nearly synchronously with valley glaciers in the tropical Andes.

Glasser et al. (2009) point the absence of a “standard” scaling method and production rate for dating tropical regions, drawing attention to the fact that different sets of reference production rates and scaling methods yield quite different results: “Zech et al. (2007) showed that a recalculation of Smith’s and Farber’s LLGM dates using the SLHL (at sea-level at high-altitude) production rate and scaling method of Lifton et al. (2005) without using the local best-fit for pressure by Farber et al. (2005) yielded ages between 22 and 25 ka, which agree with the global LGM” (Glasser et al. 2009).

YD: Glasser et al. (2009) report cosmogenic surface exposure ^{10}Be ages of 21 boulders on moraines in the Jeullesh and Tuco Valleys in Cordillera Blanca. They propose that the best approach is to calculate ages in a way that they are comparable with other existing datasets in the region, so they use the scaling systems of both Lifton et al. (2005) and Farber et al. (2005). Using Lifton scaling system, they estimated the age of the outer lateral moraines at the mouths of the valleys to be 12.4 ka (Jeullesh) and 12.5 ka (Tuco). These values fall within the published age ranges for the Younger Dryas Chronozone (YDC, 12,9-11,6 ka BP). Inside the large lateral moraines there are smaller moraine systems deposited in later stillstand or minor advances, dated to 11.3–10.7, 9.7 and 7.6 ka, covering the YDC. Using Farber´s scaling system, the dates are 14,7ka (Jeullesh) and 15 ka (Tuco) for the outer lateral moraines, and 13.4–12.7, 11.6 and 9.5 ka for the inner moraines. The paleoclimatic records of Huascarán ice cores interpreted by Thompson et al. (2003) show a number of cooling events after 14,5 ka, which Glasser et al. (2009) prefer as a reason to explain their glacier advances between 12,5 ka and 7,6 ka BP.

LIA: Solomina et al. (2007) reported the reconstruction of the chronology of LIA glacier advances. They focus on the LIA maxima through lichonometric and geomorphic studies, on the basis of an improved Rhizocarpon subgenus Rhizocarpon growth curve. They studied 66 LIA moraines of 14 glaciers in Cordillera Blanca. The main peak of glacier advance on the Pacific-facing slope of the Cordillera Blanca occurred between AD 1590 and AD 1720, triggered both by a decrease in temperature and an increase in snow accumulation according to Thompson´s ice-core data from Huascaran. Less extensive, the younger advances between AD 1780 and 1880, coincide with cooler temperatures in the ice cores.

Modern glacier fluctuations: The start of glacier retreat from advanced LIA positions is difficult to determine (Kaser, 1999). Broggi (1943) quoted information from A. Raimondi indicating that the retreat in the Cordillera Blanca had started around 1862 (Solomina, 2007), but could not be dated exactly. A first XXth century advance was reported by miners of Mina Atalante around the middle of 1920s, which reached almost the same extent as LIA. From 1930 to 1950 a retreat took place mainly due to drier conditions but also to decreasing temperatures, followed by a minor advance in the 1970s due to increasing precipitation, to retreat again faster along the XXth and XXIst centuries (Kaser, 1999). For the Cordillera Blanca it is suggested that only one-third of the glacier retreat can be attributed to the change in air temperature, and two-thirds to the variables which changed due to decreased air humidity (Kaser et al. 1997).

1.5 Glacier hazards

Glacial hazards and risks associated with glacier retreat, such as ice avalanches, new glacier lake formation and glacial lake outburst floods (GLOF), constitute a major cause of severe damage in populated mountain areas (Huggel et al., 2004). The combination of tectonic and glaciological characteristics of the Cordillera Blanca makes it a potentially threatened region (Kaser and Georges, 2003).

Peruvians have suffered the wrath of melting glaciers like no other society on earth (Carey, 2010). Many of them live directly beneath melting glaciers and unstable glacial lakes experiencing firsthand the consequences of global warming and glacier retreat. As glaciers retreat, lakes frequently formed where ice existed previously and are often dammed precariously behind weak moraines. The number of Cordillera Blanca lakes has risen dramatically from 223 in 1953 to more than 400 today (Carey, 2010) causing deadly catastrophes during the XIXth and XXth centuries mainly in the form of GLOFs. In total, more than 25.000 Peruvians have died in Cordillera Blanca glacier disasters since 1941. Table 1.1 summarizes of the glacier-related disasters in the history of Cordillera Blanca.

Table 1. 1: Glacier-related disasters in Cordillera Blanca, modified from Carey (2010)

Date	Type	Origin	Damaged area	Deaths and damages
6 Jan 1725	Avalanche/GLOF	Huandoy	Ancash destroyed	1.500 deaths
10 Feb 1869	GLOF		Monterrey	11 deaths, houses
24 Jun 1883	GLOF	Rajucolta	Macashca destroyed	deaths
22 Jan 1917	Avalanche/GLOF	Huascarán Norte	Ranrahirca and Shacsha	
13 Mar 1932	GLOF	Solterococha	Bolognesi province	
20 Jan 1938	GLOF	Artesa	Carhuaz	Ulta Canyon
13 Dec 1941	GLOF	Palcacocha (Cojup)	Huaraz	5.000 deaths Huaraz destroyed
17 Jan 1945	GLOF	Ayhuiñaraju	Chavín	Chavín and ruins destroyed
20 Jan 1950	GLOF	Jankarurish Los Cedros	Cañón del pato	200 deaths Hydroelectric plant
17 Jul 1951	GLOF	Artesoncocha	drained into Lake Parón	
28 Oct 1951	GLOF	Artesoncocha	drained into Lake Parón	
6 Nov 1952	GLOF	Milluacocha	Ishinka Canyon	Farms
18 Jun 1954	GLOF	Tullparaju	ongoing lake control project	
8 Dec 1959	GLOF	Tullparaju	ongoing lake control project	
10 Jan 1962	Avalanche	Huascarán	Ranrahirca and valley	4.000 deaths
19 dec 1962	GLOF	Tumarina	Carhuascancha Canyon	10 deaths
31 May 1970	Avalanche	Huascarán Norte	Yungay	15.000 deaths
21 Dec 1979	GLOF	Paccharuri Canyon	Vicos	Livestock killed, trail, farms
14 Feb 1981	GLOF	Sarapococha	Cajatambo	Bridge, highway
31 Aug 1982	GLOF	Milluacocha	Carhuaz	Trails and bridges
16 Dec 1987	Avalanche	Huascarán	Yungay	Livestock killed, road
20 Jan 1989	Avalanche	Huascarán	Yungay	Livestock killed, road
1991	GLOF	Lake 513	Carhuaz	Bridges and irrigation canals
Jan 1997	GLOF	Pacliashcoha	Carhuaz	Bridges, roads, pastures
20 May 1997	GLOF	Artizón Baja	Huaylas	Santa Cruz trail
2002	Lake overflow	Safuna	Pomabamba province	Livestock killed
19 Mar 2003	Lake overflow	Palcacocha		Lake security dam partially destroyed
16 Oct 2003	Avalanche	Hualcán	Carhuaz	9 glacial-ice collectors killed
11 Apr 2010	GLOF	Lake 513	Carhuaz	infrastructure, houses, agriculture and cattle

Since 1940s, scientists, engineers and government officials have undertaken several programs to gain glacier knowledge and to develop engineering projects to dam and drain glacial lakes, with the ultimate aim of preventing glacier disasters. 34 glacial lakes have been drained and dammed, and over 600 glaciers and 400 glacial lakes have been monitored since then. As a consequence, this has offered the longest glacier-climate dynamic research in the tropics. Glacier disasters affect various social groups including local urban and rural residents, scientists, engineers, water developers, government officials, and tourists (Carey, 2010). Moreover, glacier disasters mean different things for each of these groups, and this leads to the question of "who has the right to the ice and how glaciers should be managed" (Carey, 2010). Carey (2010) contends: "The history of climate change and glacier control is thus a history of power struggles-not just between humans and the physical environment, but among various social groups". Carey introduces a new concept, that of "Disaster economics", which he describes as: "the use of catastrophe to promote and empower a range of economic development interests; this development can follow both disaster and disaster prevention programs and can be private or state-owned, planned or unintentional, neoliberal or otherwise". Depending on which institution had the power over the glaciers, the studies and programs developed were either directed to understand and prevent glacier hazards, or to mainly utilitarian and economic concerns like hydroelectric production or water resources. Carey draws the attention on the fact that "sadly, electricity production was often a more compelling motivation for government disaster prevention programs than were thousands of deaths" (Carey, 2010). Table 1.2 shows a general overview of the Government Entities conducting glacier and glacial lakes projects.

Table 1. 2: Government entities conducting glacier and glacial lakes projects, modified from Carey (2010).

Year	Entity name	Agency Oversight	Government Ministry Responsible	Peruvian President
1941-1950	No specific entity	Water and irrigation	Development Division	Manuel Prado y Ugarteche
1951-1971	CCLCB	CCLCB	Development and public Works (after 1968, Agriculture)	Manuel A. Odriá
1966-1973	Division of Glaciology and Lakes Security	CPS	Energy and Mines	Juan Velasco Alvarado
1967	ING	ING	Council of Cultural development	Juan Velasco Alvarado
1973-1977	Glaciology and Lakes Security Program	Electroperú	Energy and Mines	Juan Velasco Alvarado/ Francisco Morales Bermúdez
1977-1979	Glaciology and Lakes Security Program	INGEOMIN	Energy and Mines	Francisco Morales Bermúdez
1979-1981	Glaciology and Lakes Security Program	INGEMMET	Energy and Mines	Francisco Morales Bermúdez
1981-1986	Glaciology and Hydrology Unit	Electroperú	Energy and Mines	Fernando Belaúnde Terry
1986-1990	Glaciology and Hydrology Unit	Hidrandina	Energy and Mines	Alan García Pérez
1990-1997	Glaciology and Hydrological Resources Unit	Electroperú	Energy and Mines	Alberto Fujimori
2001-2008	Glaciology and Hydrological Resources Unit	INRENA	Agriculture	Alejandro toledo
2008-	Glaciology and Hydrological Resources Unit	ANA	Agriculture	Alan García Pérez

Local urban and rural residents´ response to glacier disasters is also of relevance and had a strong effect on prevention plans. Besides engineering projects to drain and dam glacial lakes, glacier experts and government officials also proposed *hazard zoning* as a disaster prevention program. But hazard zoning programs failed every time they were developed, first after the 1941 Huaraz GLOF, secondly after the 1962 avalanche in Ranrahirca, and then after the 1970 avalanche in Yungay. Most locals ignored or opposed zoning and the fear of glacier disaster was less pressing than other socioeconomic concerns. Moreover, locals were confident in science and technology and also wanted to maintain their autonomy from the state. In consequence, they preferred glacial lake engineering rather than hazard zoning. However, this decision made them become highly dependent on the state to keep studying, monitoring, draining and damming glaciers and glacial lakes: "Population became vulnerable to climate change and glacier disasters not only because of forces beyond their control, but also because of their own actions and responses" (Carey, 2010).

By 1970s, authorities and experts were concerned about unstable Nevado Hualcán and its glacial lakes Cochca (partially drained in 1953) and Yanahuanca. They tried to relocate the village of Carhuaz but residents resisted. By mid-1980s a new glacial lake had formed: Laguna 513. At this time it was 250 m wide, 750 m long, 120 m deep, and dammed in its upper part by a dead ice-cored moraine. Draining Laguna 513 took a total of 9 years, from mid-1980s to 1994. A similar emergency situation occurred at the glacial lake on Ghiacciaio del Belvedere in the Italian-Swiss border, taking just one year from the formation of the lake to the total elimination of the threat. The supra-glacial lake on the Ghiacciaio del Belvedere developed in September 2001. Its area and volume increased very fast to reach its maximum level on the 26/27 June 2002. By early July the lake level had been lowered, and by October 2002 the lake had decreased to a size comparable to September 2001 when it formed (Kääb et al. 2004). The case on Nevado Hualcán was different. From 1988 to mid-1990s engineers lowered Laguna 513´s water level 5 m with two siphon pipes. From then, a project to construct drainage tunnels to lower the lake´s level much further was being planned when an avalanche from Hualcán triggered a GLOF in 1991. It caused minimal damage and no deaths thanks to previous engineering works but demonstrated once again the threat it represented. By 1994, engineers had drilled four drainage tunnels. This had lowered the lake enough to be dammed behind stable bedrock instead of unstable sinking moraine. From this date Laguna 513 was categorized as safe. That was until April 2010, when a new GLOF occurred.

On the 11th of April 2010 an ice avalanche detached at 5400 m from the steep SW slope of Nevado Hualcán and plunged into Laguna 513. This provoked a "push wave" that overtopped the bedrock dam and washed away the moraine material on top of it (Haeberli et al., 2010). This GLOF did not cause any deaths but did cause infrastructure damage such as regional water systems, roads, bridges, irrigation canals, houses, croplands, agroforestry lands, aquaculture farms and cattle (Carey, manuscript in preparation).

1.6 Aims and objectives

Three facts sustain the background of this project: 1) a significant portion of the world´s population, including Callejón del Huaylas' inhabitants, depend upon water released seasonally from mountain glaciers and snow (Carey, 2010); 2) glacial hazards and risks associated with glacier retreat, such as ice avalanches, new glacier lake formation and glacial lake outburst floods (GLOF), constitute a major cause of severe catastrophes in populated mountain areas (Huggel et al., 2004); and 3) tropical glaciers react faster to climate change than mid-latitude glaciers (Solomina et al., 2007), and they are a key indicator of climate change (Frey et al., 2010). The analysis of these problems, along with other environmental and social approaches will contribute to a better understanding of climate change adaptation and disaster risk reduction in Peruvian Andes. This understanding will allow government authorities, electricity producers, and local inhabitants to better decide upon their actions and responses.

The present project is focused on the third aspect mentioned above, without overshadowing the other two. The specific aims are: 1) to delimit glaciers on the SW slope of Nevado Hualcán in four different glacial phases (YD, LIA, 1962 and 2003) through moraine mapping and photointerpretation; 2) to calculate their surfaces; and 3) to calculate their ELAs. The methods include the use of geographical information technologies, particularly ESRI´s ArcGIS10 Geographical Information System (GIS). The results will contribute gathering new knowledge on the state of these glaciers in past and current glacial phases.

1.7 Organization of the Thesis

The introduction of this thesis is followed by chapter 2 that presents GIS geographical information technologies as applied to the goals of the project. The results of the analysis on the SW slope of Nevado Hualcán are described in chapter 3 and, finally, discussed in chapter 4, where I raise possible avenues of future work.

CHAPTER 2

METHODOLOGY

In this chapter, GIS geographical information technologies are presented as applied to the goals of the project. The GIS program used was ArcGIS10 in its ArcMap and ArcCatalgue environments. The materials needed for the study will be presented firstly, and then the five methodological phases of the analysis: georeferentiation, moraine mapping, glacier delimitation and surface estimation, ELA calculation, and spatial models of ELAs and accumulation and ablation zones.

2.1 Materials

In order to elaborate the moraine mapping the following materials were used:

Table 2. 1: Materials

Institution	Data	Date
IGN (Instituto Geográfico Nacional de Perú)	Aerial photographs	1962 flight
INGEMMET (Instituto Geológico Minero y Metalulgico de Perú	SPOT image and DEM	11th July 2008
Google	Google Earth images	16th July 2003
UCM-GFAM	50 m resolution contour lines	1955 (?)
UCM-GFAM	ELA AABR programmed Excel spread-sheets	
Alpenvereinskartographie	1:100.000 cartography	2006
GLCF University of Maryland	Landsat5 TM	31st May 1987 27th May 2006
USGS Earth Explorer	Landsat5 TM	21st April 1990 26th July 1996

Aerial photographs from the 1962 flight were purchased from the Peruvian institution Instituto Geográfico Nacional de Perú (IGN) and were used: 1) to elaborate the moraine mapping through the traditional method of photointerpretation using a stereoscope, and 2) to delimit glaciers in 1962.

The SPOT image and high resolution DEM were kindly provided by Peruvian institution INGEMMET. The SPOT image was mainly used as the reference image for geocoding the rest of the materials (Fig. 2.1).

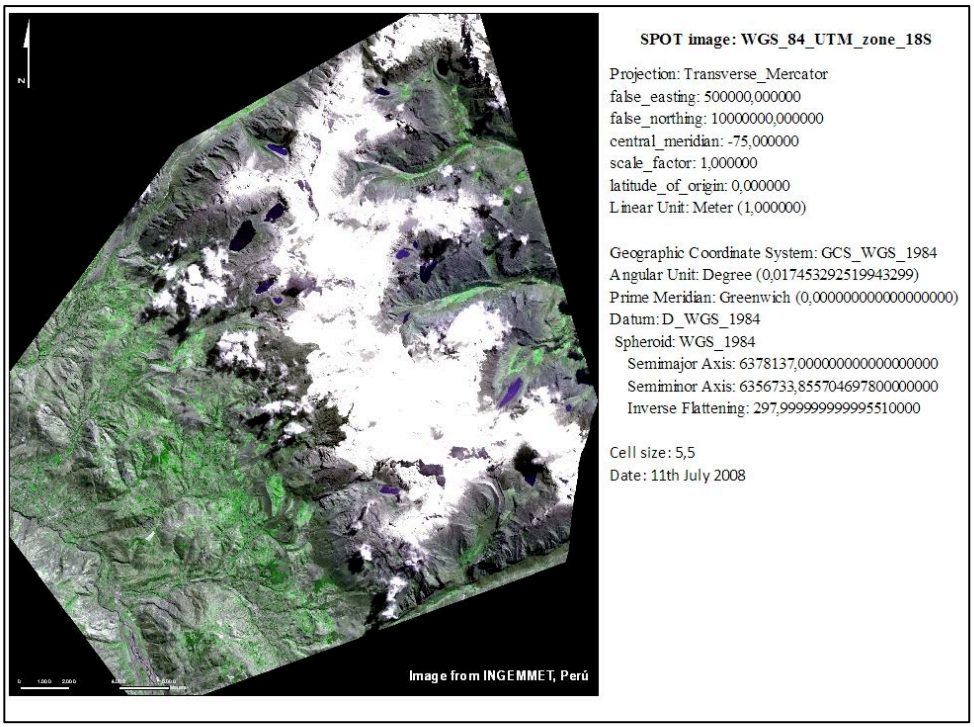

Figure 2. 1: Reference image for geocoding: Spot image.

Google Earth offers very high resolution images of the SW slope of Nevado Hualcán. In order to use these images within ArcMap10, a mosaic was elaborated that was then geocoded using the SPOT image. The mosaic was obtained by capturing images from Google Earth and combined together using Adobe Photoshop. Google Earth mosaic was the base image for: 1) delimiting glaciers in 2003; and 2) implementing the moraine mapping into the ArcGIS media.

Landsat5 TM images were downloaded from U.S Geological Survey (USGS) Earth explorer and Global Land Cover Facility (GLCF) University of Maryland services but were finally dismissed. The 50 m resolution digital contour lines of the study area were kindly provided by Dr. Úbeda. They are necessary to calculate the ELAs by the AABR method. The Microsoft Excel ELA AABR programmed spread sheets were kindly provided by Dr. Úbeda. These spread sheets are essential to calculate ELAs by this method. The topographic map scale 1:100.000 published in 2006 by the Austrian Alpine Club served as a reference but was not used in any analysis.

2.2 Georeferentiation

One potentiality of GIS software is the stacking of georeferenced data for comparison and analysis. Georeferenciation is the first step and the basis of the analysis. Thus it has to be done thoroughly to ensure the reliability of the results. The only georeferenced material

available for the project was the SPOT image which served as reference for geocoding the rest of materials (Fig. 2.1).

The aerial photographs were scanned in high resolution and converted to raster files (tiff format). Because of the conic capture of the lens, aerial photographs always incorporate a certain degree of deformation. To solve this deformation and to position the photographs into the SPOT coordinate system, they need to be geocoded. Google Earth mosaic comes from high resolution Google Earth satellite images and it does not contain any conic deformation, but nevertheless it has to be oriented to the SPOT geographical projection. Because the aim of georeferencing the aerial photographs was to delimit glaciers in 1962, only photographs corresponding to the glaciated area were orthorectified, numbers 41092 and 41093. The materials to be georeferenced (two aerial photographs and the Google Earth mosaic) will be called “raw material” in the following explanation of the geocoding process.

The geocoding procedure was carried out using the “Georeferencing” tool in ArcMap10. This implies an image-to-image registration using Ground Control Point (GCP) recognizable both on the raw material and on the SPOT image in order to attribute ground coordinates (in SPOT´s coordinate system) to the raw images. Several limitations were found in the choice of GCPs. First the difference in cell size between raw material, in high resolution raster format, and the SPOT image (5,5) subtracted accuracy to the image-to-image registration. Second, because of the time span existing between the raw material and the SPOT image, several features like glacier limits had changed and could not be taken as GCPs. GCPs were mainly located on the reference image on rocks, high peaks, and lake boundaries, and tried to cover homogeneously the image. ArcMap10 offers different georeferencing methods to calculate the geometrical transformation. Spline adjustment is the one used in this project. Spline uses the “rubber sheet method” which achieves a perfect adjustment for the GCPs, optimizing local geometrical transformation to the detriment of points far from GCPs (Andrés, 2009). For this reason, many GCPs had to be taken in order to achieve an acceptable geometrical transformation. The accuracy can be evaluated through the Root Mean Square error (RMS), which tried to be less than the pixel value in every geocoded raw material. The geometrical transformation method, the RMS error, and its corresponding planimetric error could be studied more thoroughly, and may be an issue to revise in the future. Figures 2.2, 2.3 and 2.4 illustrate the georeferencing process. Raw material is presented with 20% transparency over the SPOT image.

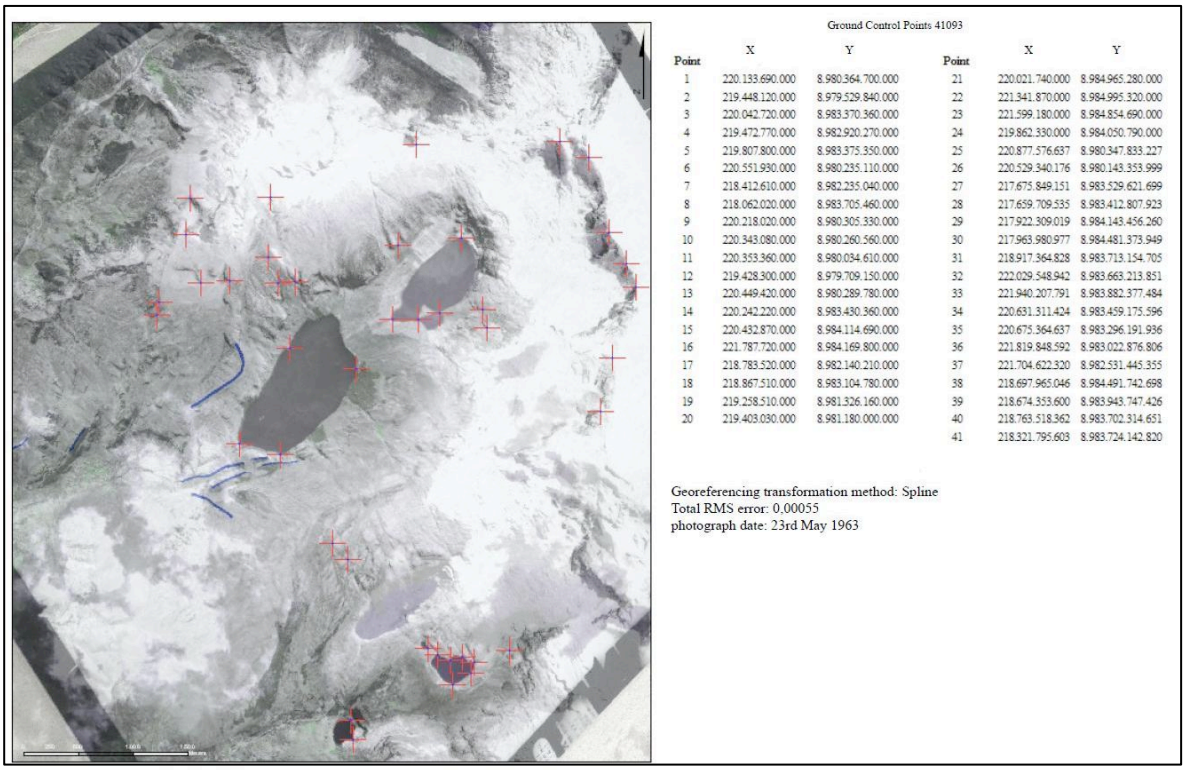

Ground Control Points 41093

Point	X	Y	Point	X	Y
1	220.133.690.000	8.980.364.700.000	21	220.021.740.000	8.984.965.280.000
2	219.448.120.000	8.979.529.840.000	22	221.341.870.000	8.984.995.320.000
3	220.042.720.000	8.983.370.360.000	23	221.599.180.000	8.984.854.690.000
4	219.472.770.000	8.982.920.270.000	24	219.862.330.000	8.984.050.790.000
5	219.807.800.000	8.983.375.350.000	25	220.877.576.637	8.980.347.833.227
6	220.551.930.000	8.980.235.110.000	26	220.529.340.176	8.980.143.353.999
7	218.412.610.000	8.982.235.040.000	27	217.675.849.151	8.983.529.621.699
8	218.062.020.000	8.983.705.460.000	28	217.659.709.535	8.983.412.807.923
9	220.218.020.000	8.980.305.330.000	29	217.922.309.019	8.984.143.456.260
10	220.343.080.000	8.980.260.560.000	30	217.963.980.977	8.984.481.373.949
11	220.353.360.000	8.980.034.610.000	31	218.917.364.828	8.983.713.154.705
12	219.428.300.000	8.979.709.150.000	32	222.029.548.942	8.983.663.213.851
13	220.449.420.000	8.980.289.780.000	33	221.940.207.791	8.983.882.377.484
14	220.242.220.000	8.983.430.360.000	34	220.631.311.424	8.983.459.175.596
15	220.432.870.000	8.984.114.690.000	35	220.675.364.637	8.983.296.191.936
16	221.787.720.000	8.984.169.800.000	36	221.819.848.592	8.983.022.876.806
17	218.783.520.000	8.982.140.210.000	37	221.704.622.320	8.982.531.445.355
18	218.867.510.000	8.983.104.780.000	38	218.697.965.046	8.984.491.742.698
19	219.258.510.000	8.981.326.160.000	39	218.674.353.600	8.983.943.747.426
20	219.403.030.000	8.981.180.000.000	40	218.763.518.362	8.983.702.314.651
			41	218.321.795.603	8.983.724.142.820

Georeferencing transformation method: Spline
Total RMS error: 0,00055
photograph date: 23rd May 1963

Figure 2. 2: Georeferencing aerial photograph 41093 over SPOT image.

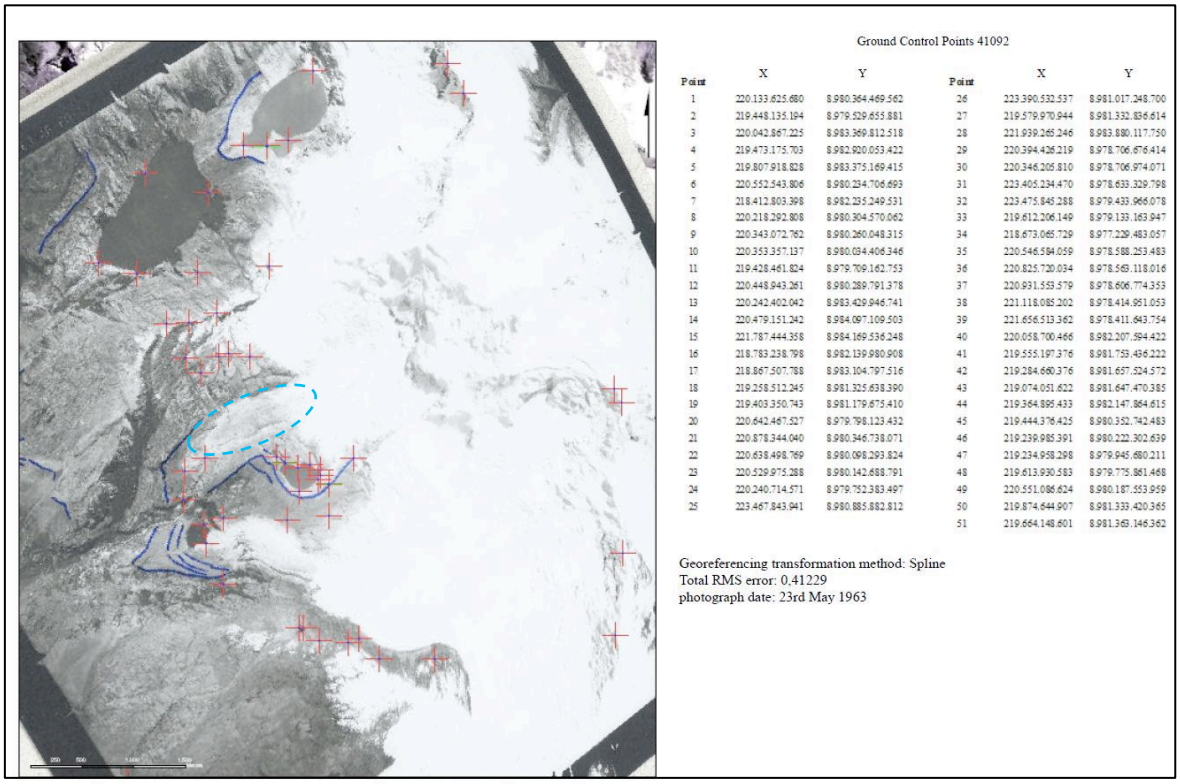

Ground Control Points 41092

Point	X	Y	Point	X	Y
1	220.133.625.680	8.980.364.469.562	26	223.390.532.537	8.981.017.248.700
2	219.448.135.194	8.979.529.655.881	27	219.579.970.944	8.981.332.836.614
3	220.042.867.225	8.983.369.812.518	28	221.939.265.246	8.983.880.117.750
4	219.473.175.703	8.982.920.053.422	29	220.394.426.219	8.978.706.676.414
5	219.807.918.828	8.983.375.169.415	30	220.346.205.810	8.978.706.974.071
6	220.552.543.806	8.980.234.706.693	31	223.405.234.470	8.978.633.329.798
7	218.412.803.398	8.982.235.249.531	32	223.475.845.288	8.979.433.966.078
8	220.218.292.808	8.980.304.570.062	33	219.612.206.149	8.979.133.163.947
9	220.343.072.762	8.980.260.048.315	34	218.673.065.729	8.977.229.483.057
10	220.353.357.137	8.980.034.406.346	35	220.546.584.059	8.978.588.253.483
11	219.428.461.824	8.979.709.162.753	36	220.825.720.034	8.978.565.118.016
12	220.448.943.261	8.980.289.791.378	37	220.931.553.579	8.978.606.774.353
13	220.242.402.042	8.983.429.946.741	38	221.118.085.202	8.978.414.951.053
14	220.479.151.242	8.984.097.109.503	39	221.656.513.362	8.978.411.643.754
15	221.787.444.358	8.984.169.536.248	40	220.058.700.466	8.982.207.594.422
16	218.783.238.798	8.982.139.980.908	41	219.555.197.376	8.981.753.436.222
17	218.867.507.788	8.983.104.797.516	42	219.284.660.376	8.981.657.524.572
18	219.258.512.245	8.981.325.638.390	43	219.074.051.622	8.981.647.470.385
19	219.403.350.743	8.981.179.675.410	44	219.364.895.433	8.982.147.864.615
20	220.642.467.527	8.979.798.123.432	45	219.444.376.425	8.980.352.742.483
21	220.878.344.040	8.980.346.738.071	46	219.239.985.391	8.980.222.302.639
22	220.638.498.769	8.980.098.293.824	47	219.234.958.298	8.979.945.680.211
23	220.529.975.288	8.980.142.688.791	48	219.613.930.583	8.979.775.861.468
24	220.240.714.571	8.979.752.383.497	49	220.551.086.624	8.980.187.553.959
25	223.467.843.941	8.980.885.882.812	50	219.874.644.907	8.981.333.420.365
			51	219.664.148.601	8.981.363.146.362

Georeferencing transformation method: Spline
Total RMS error: 0,41229
photograph date: 23rd May 1963

Figure 2. 3: Georeferencing aerial photograph 41092 over SPOT image. Laguna 513 (blue dashed line) was still a glacier.

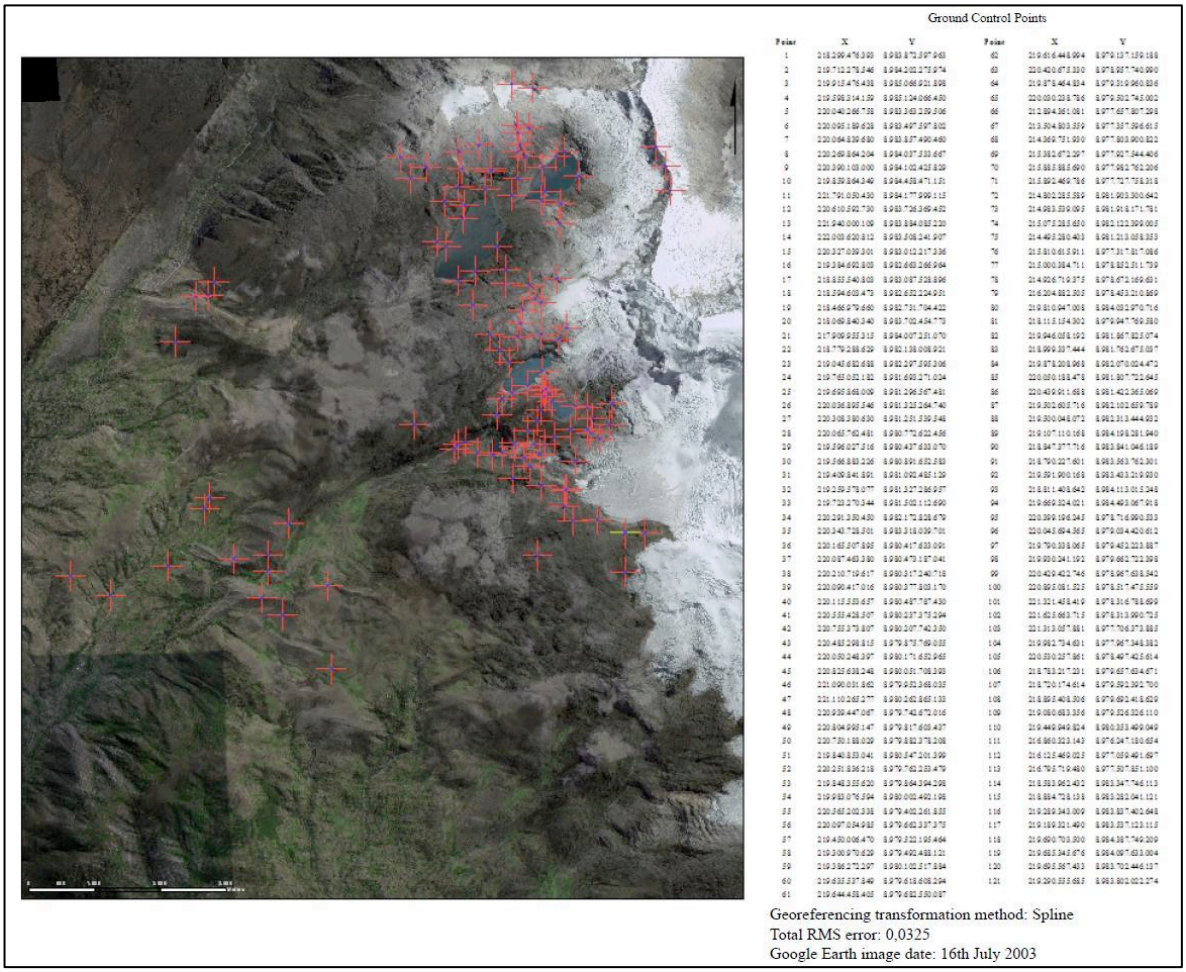

Figure 2. 4: Georeferencing Google Earth over SPOT image

2.3 Moraine mapping

Once the reference images were properly geocoded, the first step in the process of reconstructing Ice Age glaciers is to establish the geometry of the paleo-glaciers from which other characteristics and mechanisms can be deduced (Haeberli, 2010). One major point is to reconstruct the geometry of ancient glaciations based on geomorphological traces focusing on moraines as a clearly recognizable element of these traces.

Moraine mapping is divided in two main phases: 1) traditional photointerpretation of moraine cartography methods; 2) moraine cartography in ArcMap environment and relative dating.

Moraines of the SW slope of Nevado Hualcán were identified firstly by using a stereoscope and mapped over acetate paper covering the original aerial photographs. Google Earth was also used as a support tool offering very high resolution images and a 3D display. The aerial photographs correspond to the 1962 flight. However, the photographs corresponding to the glaciated area are marked as "23rd May 1963". For the delimitation of glaciers it was

assumed that they corresponded to 1962 glacier limits. A summary of the aerial photographs can be found in Annex 1.

Once moraines were identified by the photointerpretation method, they were digitalized over the georeferenced Google Earth mosaic in ArcMap10 using the "Editor" tool. A database was automatically associated to the moraine layer, where a new field called "Period" was added. This field was to be completed by the relative dating of each moraine and was the base to create the legend of the moraine cartography. The options in ArcMap10 allowed determining a qualitative color range following a filed value in the attribute table. The field "Period" was the value by which the colors were classified. The color range was chosen amongst the existing colors in ArcMap10 and from the "ColorBrewer2.0" web service. The RGB color codes for each glacial phase are shown in table 2.2

Table 2. 2: RGB Colors attributed to the moraines classified by their relative dating.

Period	RGB	Color
preLLGM	166 - 54 - 3	
LLGM	230 - 85 - 13	
postLLGM	255 - 211 - 127	
YD	255 - 170 - 0	
postYD	255 - 255 - 190	
LIA	230 - 230 - 0	
XXth century	255 - 255 - 255	
Unclassified	168 - 112 - 0	

Dating of glacial deposits like moraine boulders has been used to develop glacial chronologies. For this study, the relative dating of the selected seven glacial phases mapped in the SW slope of Nevado Hualcán was achieved through compiling literature from the chronologies published so far for the Cordillera Blanca or close regions. Table 2.3 shows the reference publications from which relative dating of moraines were established and figure 2.5 shows the final legend of the moraine cartography.

Table 2. 3: Reference publications for relative dating of moraines. CB: Cordillera Blanca.

Period	Reference publications	Location	Dating method
preLLGM	Farber et al. (2005) Smith et al. (2005)	Quebradas Cojup, Rurec, Laca and Queshque (CB)	^{10}Be exposure ages (Farber scaling system)
LLGM		Junin region (200 km from CB)	^{10}Be exposure ages
postLLGM			
YD	Glasser et al. (2009)	Jeullesh and Tuco valleys (CB)	^{10}Be ages (Lifton scaling system)
postYD			
LIA	Solomina et al. (2007)	several CB locations	Lichonometry (Rhizocarpon growth curve)
XXth century	Kaser (1999)		review

Several moraines were not classified. They belong to a section of the study area where mass movements and landslides have altered the valley´s morphology and will need a more complex geomorphological interpretation which could be reached in further research, through landform identification and absolute dating studies.

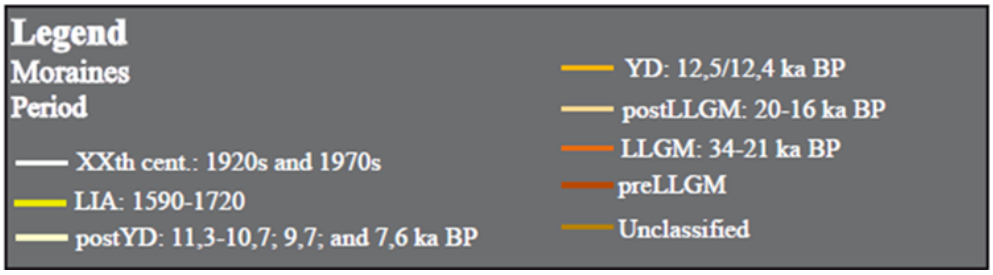

Figure 2. 5: Legend for the moraine cartography.

Moraine mapping was the basis from which to delimit paleo-glaciers in the YD and LIA glacial phases. Future research may involve absolute dating chronology reconstruction of the moraines in order to validate the relative dating presented here.

2.4 Glacier delimitation and surface calculation

The calculation of the surface of glaciers required establishing their limits. Delimitation of current glaciers was based on the aerial photographs and the Google Earth mosaic served. For paleo-glaciers, moraine mapping was used as a geomorphological reference of the traces they left behind.

2.4.1 Scope

There are several methods to delimit modern glaciers from satellite images, which allow distinguishing snow from ice. These methods were not used because satellite images were discarded for glacier delimitation. However, they may be very useful in future studies of glacier fluctuations and glacial cover mapping. Current glaciers were not delimited in single glacier apparatus because this would require field work that was out of the scope of the present work. Thus, glaciers were divided in main apparatus. As for paleo-glacier delimitation, the most ancient glacial phase analyzed in this project was the YD glacial phase. There is a sector down-valley from this phase, unclassified in the moraine mapping, where mass movement, landslides and glacial landforms may be easily misinterpreted because sediments and landforms produced by mass movement and glacial processes can look very similar (Benn et al., 2005). This section requires further and more complex geomorphological interpretation.

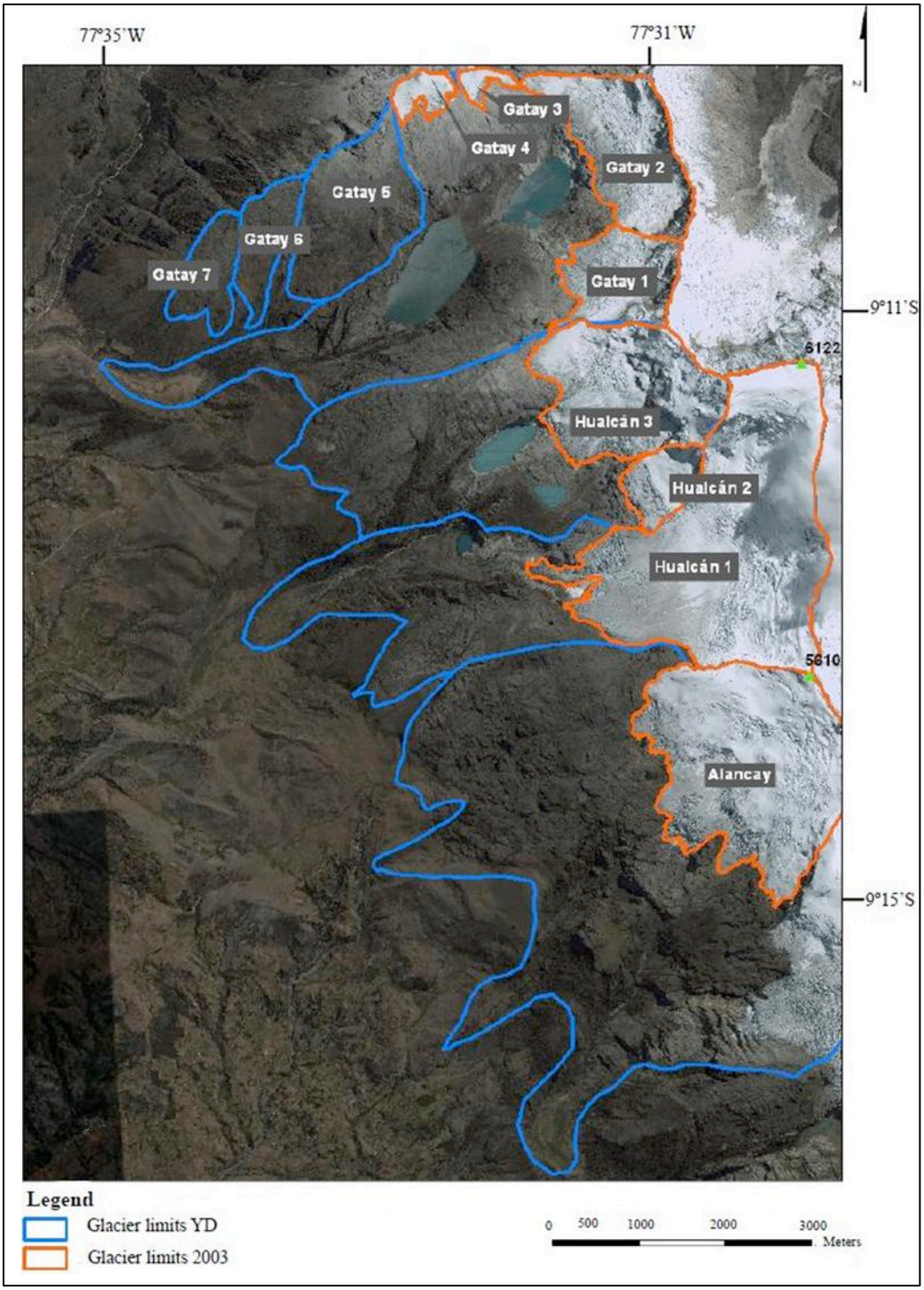

Figure 2. 6: Names given to glaciers over Google Earth mosaic.

2.4.2 Current glaciers

Google Earth mosaic images are from the 16th July 2003, which corresponds to the dry season. As a consequence, there was no snow over glacial ice and glaciers were clearly

recognizable. The aerial photographs corresponding to the glaciated area (numbers 41092 and 41093) were taken in the month of May. A layer of snow covers high altitudes and this could mislead the delimitation of glaciers. Therefore, a careful interpretation of the photographs had to be done with the help of the stereoscope. Glacier limits in 1962 and 2003 were digitalized in ArcMap10 using the "Editor" tool, and a database was automatically associated to each glacier polygon. The new fields added to the database were "NºGlacier", "Name" and "Areakm2" and were completed as each polygon was digitalized (see figure 2.5 for the names given to glaciers). The surface of each glacier was automatically calculated using the "Calculate Geometry" tool form the attribute table. The aerial photographs purchased did not cover glacier Alancay. An estimation of its surface had to be calculated by adding to Alancay´s surface in 2003 the mean of the surface differences from every glacier between 2003 and 1962. Table 2.4 explains this estimation. Glacier limits were used to calculate their ELAs.

Table 2. 4: Estimation of glacier Alancay´s surface in 1962.

Glacier	Surface (km²)		Difference
	1962	2003	
H1	6,936	6,538	0,398
H2	0,843	0,626	0,217
H3	3,541	2,762	0,779
G1	1,677	1,274	0,403
G2	2,368	2,071	0,296
G3	0,548	0,156	0,392
G4	0,550	0,291	0,259
G5	0,370	0	0,370
A		4,836	
Mean surface differences 1962-2003:			0,389
Surface estimation Alancay 1962:			*5,226*

2.4.3 Paleo-glaciers

Paleo-glaciers were reconstructed from the geomorphological traces they left behind (Haeberli, 2010). Moraines are a clearly recognizable element of these traces so the moraine mapping was used as the main reference to decide upon the limits of paleo-glaciers. The upper limits were considered to be the same for all glaciers in their different glacial phases, following the upper limits from 2003. The same fields as for current glaciers were added to the paleo-glaciers´ database ("NºGlacier", "Name" and "Areakm2").

LIA glacier limits were digitalized following LIA moraines, which were identified as the first prominent and fresh moraines after the 1962 glacier limits. In many cases they dam a glacial lake. Glaciers Gatay2, Hualcán1 and Hualcán3, dam lakes Checquiacocha, Rajupaquinan, and Cochca and 513 respectively. This maximum LIA limits were reached between 1590 and 1720 following the chronology reconstruction proposed by Solomina et

al. (2007) from lichonometric and geomorphic studies. Moraines placed between LIA and 1962 limits were considered to be modern XXth century maximum advances reached mostly in mid-1920s and, to a minor extent, in 1970s.

YD glacier limits were digitalized following the YD moraines, which were identified as the first prominent moraines down-valley from LIA limits. Glaciers appearing in previous phases as separate apparatus were considered one joined apparatus for the YD glacial phase. Following the report presented by Glasser et al. (2009) on cosmogenic ^{10}Be exposure ages, the moraines identified as YD in the SW slope of Nevado Hualcán correspond to the outer lateral moraines at the mouths of Jeullesh and Tuco valleys. Thus, the relative dating of YD moraines in Nevado Hualcán was considered to be 12,4-12,5 ka BP. Inside the large lateral moraines, between YD and LIA limits, there are smaller moraine systems deposited in later stillstand or minor advances, dated to 11.3–10.7, 9.7 and 7.6 ka (Glasser et al., 2009).

This geometric reconstruction inferred from geomorphological features, served to estimate the ELAs of LIA and YD glaciers.

2.5 ELAs AABR

ELA stands for Equilibrium Line Altitude. It is the theoretical line dividing the accumulation zone and the ablation zone. Traditional definitions of ELA refer to the altitude where b_n=0, where b_n is the net mass balance at the end of the ablation season (Benn et al. 2005). This definition was developed for mid- and high-latitude glaciers, but is less obviously applicable to tropical glaciers where there is year-round ablation. Kaser et al. (1990) follow the definition of the mass balance year as extending from one entire glacier mass minimum to the next, so they assume that the end of the dry season is the end of the mass balance year. Osmaston (2005) uses the term ELA referring to a glacier in a hypothetical balanced state, i.e. when the net mass balance of the whole glacier is or would be zero.

Several methods for reconstructing ELAs and paleoELAs are described in Úbeda (2010), who among geomorphologic procedures of ELA reconstruction distinguishes morphometric (only for paleo-glaciers) and statistical methods (for current and former glaciers). Statistical methods take into account the hypsometry, which is the detailed distribution of surface area with respect to altitude of glaciers. They are based on the principle that parts of a glacier which are far above or below the ELA have greater spot net balances and more influence on the total mass balance of a glacier and on the ELA, than those which are close (Osmaston, 2005).

Within statistical methods, the Area x Altitude Balance Ratio (AABR) method is considered to be rigorous and reliable (Osmaston, 2005; Benn et al. 2005). ELA results obtained through this method were chosen by Úbeda (2010) as reference to compare other morphometric and statistical methods. The present project will focus on the application of

the AABR method to calculate the ELAs and paleoELAs of glaciers in the SW slope of Nevado Hualcán.

Osmaston (2005) offers a detailed explanation of AABR method including the procedure to use a proposed programmed Microsoft Excel spread sheet. The AABR method is described as follows: "(AABR) is based on the principle of weighting the mass balance in areas far above or below the ELA by more than in those close to it. However this is then refined by providing for different linear slopes of the mass balance/altitude curve above and below the ELA. Many glaciers conform roughly to this specification, and it serves as a useful first approximation for former glaciers for which there is no a priori knowledge about their mass balance. It was developed by Osmaston who originally termed it the Area-Height-Accumulation method for use on East African mountain glaciers." (Osmaston, 2005).

The AABR method requires knowledge of the position of the margin of a glacier (glacier delimitation) and contour data for its surface: 50 m resolution contour lines transformed into contour belts, explained in point 2.5.1. The area and mean altitude of successive contour belts of each glacier surface was determined. The original 50 m contour lines were appropriately adjusted for former glaciers based on a hypothetical reconstruction of their ice surface and volume. What follows will explain the procedure to create the contour belts, to adjust contour lines for paleoglaciers, and finally the calculation of ELA AABR both for current and former glaciers.

2.5.1 ELAs AABR: 1962 and 2003

As mentioned above, the method of reconstructing current glaciers´ ELAs AABR requires knowledge on the position of the margin of a glacier (glacier delimitation) and contour data for its surface (50 m resolution contour lines transformed into contour belts). Glacier delimitation was achieved in previous phase 2.4. The next step was the generation of the contour belt layer. A contour belt is the area between two contour lines. While contour lines are presented in a polyline shapefile, contour belts have to be contained in a polygon shapefile in order to calculate each surface area. For this purpose, the 50 m resolution digital contour polyline shapefile was the base material to create the contour belt polygon shapefile. All the steps were carried out using ArcGIS10 in its ArcMap10 and ArcCatalogue10 environments.

The original digital contour lines cover a much wider area than that needed for this study. A new polygon ("StudyArea.shp") representing the area of study was created in ArcCatalogue. The ArcMap10 tool called "Intersect" (ArcTooBox-Analysis Tools-Overlay-Intersect) computes a geometric intersection of the input features, where the features or portion of features which overlap in all layers were written to the output feature. The input features were the original contour line shapefile and the new polygon representing the area of interest. The output feature was a polyline shapefile containing the contour lines of the study area ("TopographyArea.shp").

Table 2. 5: Summary of the steps followed to obtain the contour belts of each glacier.

Step	Tool	Input	Output
1	Intersect	contour lines	contour lines of the study area
		polygon of the study area	
2	Feature to Plolygon	contour lines of the study area	contour belts of the study area
		polygon of the study area	
3	Clip	contour belts of the study area	contour belts of the selected glacier
		Clip feature: selected glacier polygon	

The tool “Feature to Polygon” creates a shapefile containing polygons generated from areas enclosed by input lines or polygon features. Using as input features the new polyline contour lines shapefile of the study area (“TopographyArea.shp”) and the polygon shapefile representing the study area (“StudyArea.shp”), the new output polygon shapefile contains the contour belts (“BeltsZArea.shp”). On the attribute table of this new shapefile, three fields must be added: “Interval”, “MeanZ” and “Area” These fields were completed using the “Editor” tool containing respectively the altitude interval of each contour belt, its mean altitude and its area. The area, in m², was automatically calculated using the “Calculate Geometry” tool in the attribute table. This magnitude (m²) will be used for all the ELA calculation process. Figure 2.7 illustrates this first step.

Once the contour belts shapefile was completed, the next step was to obtain the contour belts of each glacier in each date. The “Clip” tool (ArcTooBox-Analysis Tools-Extract-Clip) allows to cut out a piece of one feature (input feature) using another feature (clip feature). The input feature used was the contour belts shapefile (“BeltsZArea.shp”) and the clip feature was the polygon representing a glacier. One single glacier was selected and used as clip feature, and the process had to be repeated for each glacier in every glacial phase. The output resulting features were the polygon shapefiles containing the contour belts in each glacier (e.g. “BeltsZH1.shp”, “BeltsZH2.shp”, “BeltsZH3.shp”…; see Fig. 2.8). The filed “Area” had to be recalculated. The attribute tables of each glacier´s contour belts were exported as a .dbf table which could be opened on a Microsoft Excel sheet. This information was used in the ELA AABR programmed sheets.

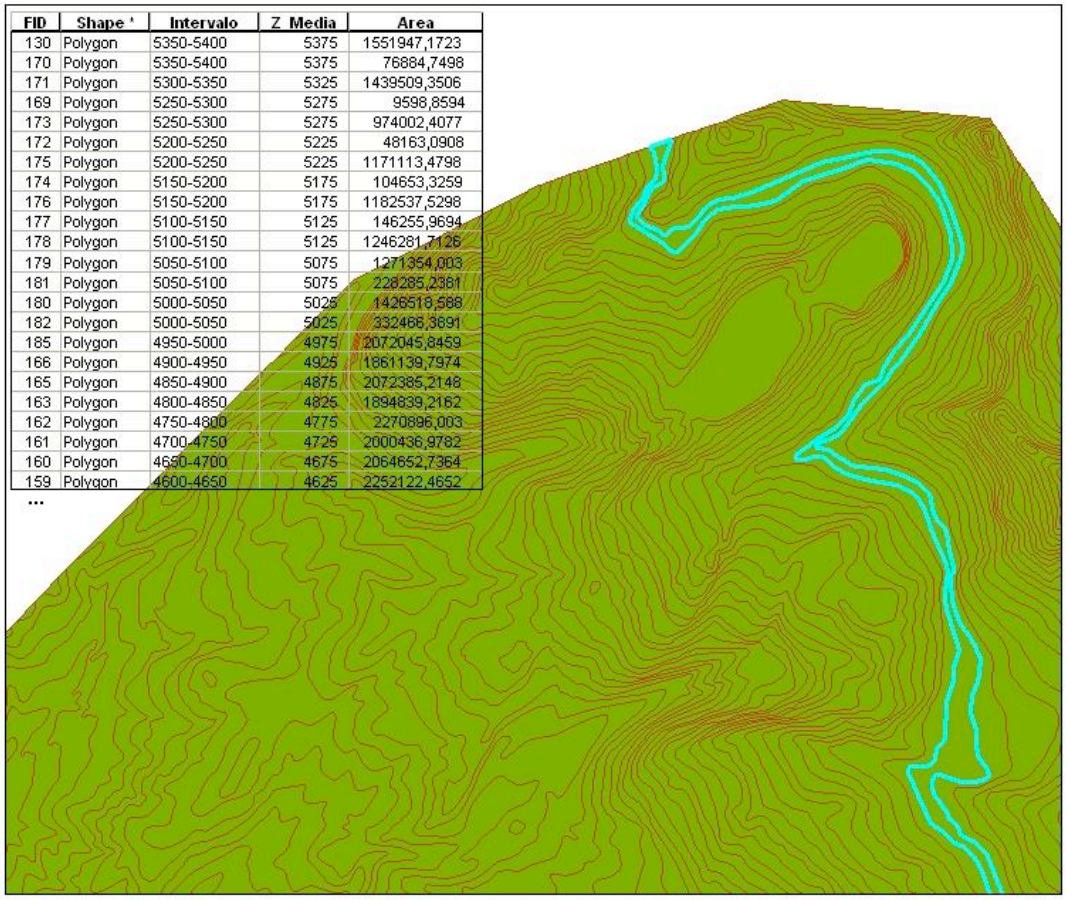

FID	Shape *	Intervalo	Z_Media	Area
130	Polygon	5350-5400	5375	1551947,1723
170	Polygon	5350-5400	5375	76884,7498
171	Polygon	5300-5350	5325	1439509,3506
169	Polygon	5250-5300	5275	9598,8594
173	Polygon	5250-5300	5275	974002,4077
172	Polygon	5200-5250	5225	48163,0908
175	Polygon	5200-5250	5225	1171113,4798
174	Polygon	5150-5200	5175	104653,3259
176	Polygon	5150-5200	5175	1182537,5298
177	Polygon	5100-5150	5125	146255,9694
178	Polygon	5100-5150	5125	1246281,7126
179	Polygon	5050-5100	5075	1271354,003
181	Polygon	5050-5100	5075	228285,2381
180	Polygon	5000-5050	5025	1426518,588
182	Polygon	5000-5050	5025	332466,3891
185	Polygon	4950-5000	4975	2072045,8459
166	Polygon	4900-4950	4925	1861139,7974
165	Polygon	4850-4900	4875	2072385,2148
163	Polygon	4800-4850	4825	1894839,2162
162	Polygon	4750-4800	4775	2270896,003
161	Polygon	4700-4750	4725	2000436,9782
160	Polygon	4650-4700	4675	2064652,7364
159	Polygon	4600-4650	4625	2252122,4652

...

Figure 2. 7: Contour belts and a section of its attribute table. Contour belt 4900-4950 m is selected.

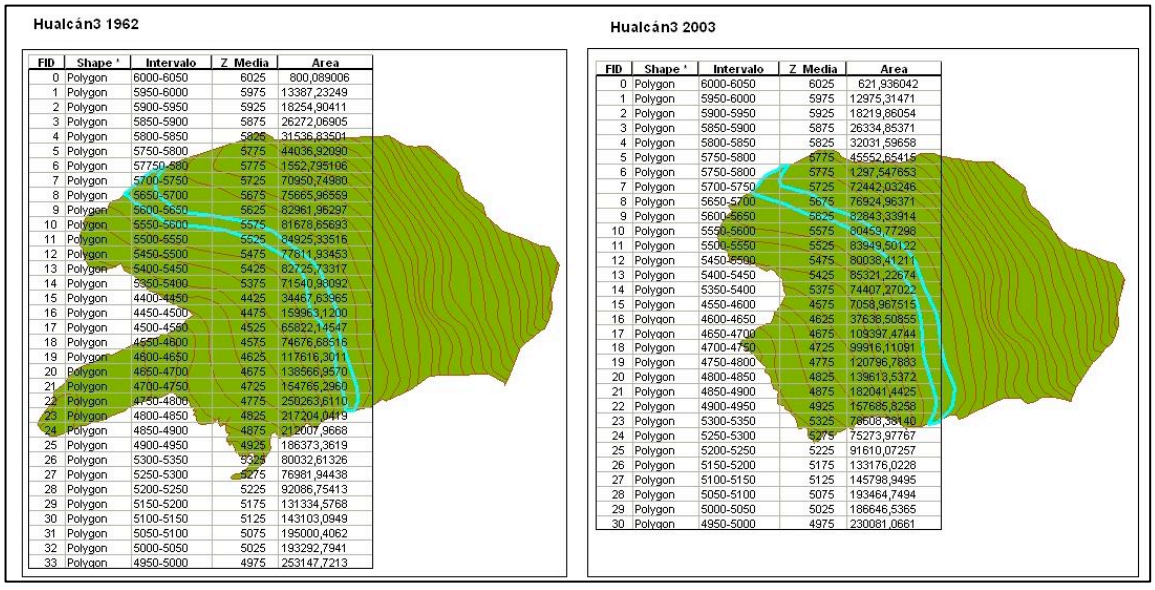

Hualcán3 1962

FID	Shape *	Intervalo	Z_Media	Area
0	Polygon	6000-6050	6025	800,089006
1	Polygon	5950-6000	5975	13387,23249
2	Polygon	5900-5950	5925	18254,90411
3	Polygon	5850-5900	5875	26272,06905
4	Polygon	5800-5850	5825	31536,83501
5	Polygon	5750-5800	5775	44036,92090
6	Polygon	5700-5750	5725	70950,74980
7	Polygon	5650-5700	5675	75665,96569
8	Polygon	5600-5650	5625	82961,96297
9	Polygon	5550-5600	5575	81678,65693
10	Polygon	5500-5550	5525	84925,33516
11	Polygon	5450-5500	5475	77811,93453
12	Polygon	5400-5450	5425	82725,73317
13	Polygon	5350-5400	5375	71540,90092
14	Polygon	4400-4450	4425	34467,63965
15	Polygon	4450-4500	4475	159963,1200
16	Polygon	4500-4550	4525	65822,11647
17	Polygon	4550-4600	4575	74676,68516
18	Polygon	4600-4650	4625	117616,3011
19	Polygon	4650-4700	4675	138566,9570
20	Polygon	4700-4750	4725	154765,2960
21	Polygon	4750-4800	4775	250263,6110
22	Polygon	4800-4850	4825	217204,0419
23	Polygon	4850-4900	4875	212007,9668
24	Polygon	4900-4950	4925	186373,3619
25	Polygon	5300-5350	5325	80032,61326
26	Polygon	5250-5300	5275	76981,94438
27	Polygon	5200-5250	5225	92086,75413
28	Polygon	5150-5200	5175	131334,5768
29	Polygon	5100-5150	5125	143103,0949
30	Polygon	5050-5100	5075	195000,4062
31	Polygon	5000-5050	5025	193292,7941
32	Polygon	4950-5000	4975	253147,7213
33	Polygon	4950-5000	4975	253147,7213

Hualcán3 2003

FID	Shape *	Intervalo	Z_Media	Area
0	Polygon	6000-6050	6025	621,936042
1	Polygon	5950-6000	5975	12975,31471
2	Polygon	5900-5950	5925	18219,86054
3	Polygon	5850-5900	5875	26334,85371
4	Polygon	5800-5850	5825	32031,59658
5	Polygon	5750-5800	5775	45552,65415
6	Polygon	5750-5800	5775	1297,547653
7	Polygon	5700-5750	5725	72442,03246
8	Polygon	5650-5700	5675	76924,96371
9	Polygon	5600-5650	5625	82843,33914
10	Polygon	5550-5600	5575	80459,77298
11	Polygon	5500-5550	5525	83949,50122
12	Polygon	5450-5500	5475	80038,41211
13	Polygon	5400-5450	5425	85321,22674
14	Polygon	5350-5400	5375	74407,27022
15	Polygon	4550-4600	4575	7058,967515
16	Polygon	4600-4650	4625	37638,50855
17	Polygon	4650-4700	4675	109397,4744
18	Polygon	4700-4750	4725	99916,11091
19	Polygon	4750-4800	4775	120796,7883
20	Polygon	4800-4850	4825	139613,5372
21	Polygon	4850-4900	4875	182041,4425
22	Polygon	4900-4950	4925	157685,8258
23	Polygon	5300-5350	5325	78608,38140
24	Polygon	5250-5300	5275	75273,97767
25	Polygon	5200-5250	5225	91610,07257
26	Polygon	5150-5200	5175	133176,0228
27	Polygon	5100-5150	5125	145798,9495
28	Polygon	5050-5100	5075	193464,7494
29	Polygon	5000-5050	5025	186646,5365
30	Polygon	4950-5000	4975	230081,0661

Figure 2. 8: Example of contour belts and their complete attribute tables for Hualcán 3 in 1962 and 2003. Contour belt 4900-4950 m is selected in both figures.

From this stage, ELA AABR calculations were completed in Microsoft Excel environment. Osmaston (2005) describes in detail a procedure for ELA AABR using Excel programmed spread sheets. The basis of this method lays on the equation presented by Sisson (1978, 1980) and taken by Osmaston (2005):

$$\mathrm{ELA} = \quad \mathrm{Z} * \mathrm{A} / \quad \mathrm{A}.$$

The application of this equation in the Excel spread-sheets is explained below. The results obtained need to be weighted by different Balance Ratio (BR) values.

The following points proposed by Osmaston (2005) were considered and adapted to this work:

1. Check correct operation of spread sheet with trial data.

2. Check that contour table will cover glaciers to be examined (insert rows if necessary to cover all contour belts) and that VI (equidistance between contour lines, column B) is correct (here, 50 m).

3. Enter contour belt area table for glacier 1 (in the example, Hualcán3). These are the fields “ZInterval”, “Mean Z” and “Area m²” (columns C, D and E) exported from the attribute table of each glacier from ArcMap10.

4. Enter, in column H, the altitude of the first trial reference contour line immediately below the first ELA value obtained through the AA ELA shortcut method, this is applying Sisson´s equation (in the example this ELA value is in F18).

5. Enter BR=1 (columnG) and check correct operation (“TRUE” in H18).

6. Record ELA VALUE in column M (AABR ELA for other BRs interpolated between contours, in example M22). Copy this result to the results table (C26)

7. Enter in succession a series of BR values (e.g. 1, 1.5, 2, 2.5, 3) and record the ELA for each as in steps 5 and 6. Ratios can be selected by a priori knowledge of what is likely; most glaciers are likely to have BRs of 1.5–3.5, though on a debris-covered one it may be less than 1.

8. Repeat for the other glaciers.

These eight steps are shown in Table 2.6 and can be followed through the same numbers and colors as used above. A similar table was obtained for each glacier.

Table 2. 6: The main section of an AABR spread-sheet for glacier Huacán3 in 1962.

	A	B	C	D	E	F	G	H	I	J	K	L	M	N
1	GLACIER	Contour vertical interval (VI) (2)	Z Interval (3)	Mean Z (3)	Area m² (3)	Z media x Area	Balance Ratio (BR) (7)	ELA trial Reference contour (4) (1)	Belt area x Alt above ref. contour (1)	Area x Alt x Balance Ratio for contour (1)	ELA trial Reference contour (2)	Belt area x Alt above ref. contour (2)	Area x Alt x Balance Ratio for contour (2)	...
2	Hulacán 3	50,0	6000-6050	6025	800,089	4820536	1 (5)	5000 (4)	4820536	4820536	5050	4820536	4820536	
3	1962		5950-6000	5975	13387,232	79988714			79988714	79988714		79988714	79988714	
4			5900-5950	5925	18254,904	108160307			108160307	108160307		108160307	108160307	
5			5850-5900	5875	26272,069	154348406			154348406	154348406		154348406	154348406	
6			5800-5850	5825	31536,835	183702064			183702064	183702064		183702064	183702064	
7			57750-5800	5775	1552,795	8967392			8967392	8967392		8967392	8967392	
8			5750-5800	5775	44036,921	254313218			254313218	254313218		254313218	254313218	
9			5700-5750	5725	70950,750	406193043			406193043	406193043		406193043	406193043	
10			5650-5700	5675	75665,966	429404355			429404355	429404355		429404355	429404355	
11			5600-5650	5625	82961,963	466661042			466661042	466661042		466661042	466661042	
12			5550-5600	5575	81678,657	455358512			455358512	455358512		455358512	455358512	
13			5500-5550	5525	84925,335	469212477			469212477	469212477		469212477	469212477	
14			5450-5500	5475	77811,935	426020342			426020342	426020342		426020342	426020342	
15			...	...	...	...			...	...		...	...	
16	TOTALS				3540809	17852603200			148557217,2	148557217,2		-28483242,65	-28483242,65	
17	RESULTS													
18	AA ELA (median alt x area, shortcut method) (4)=					5041 (4)	CHECK =	TRUE (5)						
19	AABR ELA for BR=0 (if exact contour) =													
20	AABR ELA for BR=1 (interpolated between contours) =											5041,955725		
21	AABR ELA for other BRs (if exact contour) =													
22	AABR ELA for other BRs (interpolated between contours) (6) =												5041 (6)	
23														
24			RESULTS											
25			BR=1	BR=1,5	BR=2,0	BR=2,5	BR=3							
26	Hulacán 3	AABR ELA for	5041 (6)	5015	5052	5078	5097							
27														
28					(7)									

Column H contains the altitude of the first reference contour line immediately below the first ELA value obtained through Sisson´s equation (AA ELA shortcut method). Column K represents the contour line immediately above the reference contour line in column H. The full table extends to column AK, repeating columns K, L, M for successive values of trial ELA, until the columns AI, AJ and AK are reached for trial number 10.

Sisson´s equation is integrated in the Excel spread-sheet through columns F and E and their total appears in row 16. Sisson´s equation is:

$$\mathrm{ELA} = \quad \mathrm{Z} * \mathrm{A} / \quad \mathrm{A}$$

Column F calculates Z*A; column E calculates A; F16 contains $\mathrm{Z} * \mathrm{A}$; E16 contains A; and F18 is the value of ELA through Sisson´s equation (in this case F16/E16).

After obtaining the results for all glaciers, data were analyzed using a second spread-sheet which includes the ELA results of all glaciers weighted by different BR. In this new summary sheet the following steps were carried out adapted from Osmaton (2005):

9. Enter results in a spread sheet for displaying them and calculating the mean and standard deviation of the estimated ELAs for each BR value.

10. Select the BR with the lowest standard deviation, which indicates the ELA with the best statistical probability of being correct (explained in point 2.6).

11. Plot the ELAs on a map to see if they show any pattern of grouping, clines or sloping surfaces and re-analyze the data accordingly (see point 2.6).

Table 2.7: Validation spread sheet for estimating the standard deviations of ELAs of a group of glaciers for different BRs.

QUEBRADA HUALCÁN	BR=1,0	**BR=1,5**	BR=2,0	BR=2,5	BR=3,0
Hulacán 1	5283	5275	5315	5343	5363
Hualcán 2	5108	5112	5126	5135	5142
Hualcán 3	5152	5200	5233	5255	5272
Mean (9)	5181	**5196**	5225	5244	5259
Standard deviation (9)	91	**82**	95	104	111
QUEBRADA GATAY	**BR=1**	BR=1,5	BR=2,0	BR=2,5	BR=3
Gatay 1	5174	5159	5181	5197	5208
Gatay 2	4989	4962	4955	4968	4977
Gatay 3	5024	5015	5009	5005	5002
Gatay 4	5110	5102	5110	5115	5119
Mean (9)	**5074**	5060	5064	5071	5077
Standard deviation (9)	**84**	88	101	105	107
QUEBRADA ALANCAY	BR=1	BR=1,5	BR=2,0	BR=2,5	BR=3
	5150	5188	5213	5231	5244
VERTIENTE SW	**BR=1 (10)**	BR=1,5	BR=2,0	BR=2,5	BR=3
Mean (9)	**5124 (10)**	5127	5143	5156	5166
Standard deviation (9)	**90 (10)**	102	119	127	133

2.5.2 paleoELAs AABR: YD and LIA

The same procedure as described above was carried out to calculate paleoELAs AABR for LIA and YD glaciers. This consisted first to create the contour belts in ArcMap10, and then to calculate the ELAs AABR with Microsoft Excel spread-sheets.

In the case of former glaciers, a previous step was required before creating the contour belts: the original contour lines needed to be modified in order to represent paleo-glaciers. Glaciers charted as YD and LIA do not exist anymore, neither when the digital contour lines were created. For this reason, what in current topography appears as glacier eroded valleys, it is assumed that in former times were filled with glaciers. Thus, the contour lines should be adjusted to a hypothetical reconstruction of the ice surface and volume. The procedure is laborious as each contour line must be modified. The same paleo-topography was used for LIA and YD glaciers. The reconstruction of paleo-topography was completed with ArcMap10.

Table 2. 8: Summary of the steps followed to obtain the hypothetical reconstructed paleo-topography of the study area.

Step	Tool	Input	Output
1	Clip	original contour lines of the study area	original contour lines inside YD glacier limits
		Clip feature: YD glacier limits	
2	Editor	original contour lines inside YD glacier limits	reconstructed contour lines inside YD glacier limits
3	Erase	original contour lines of the study area	contour lines of the study area without YD glacier limits
		Erase feature: YD glacier limits	
4	Merge	contour lines of the study area without YD glacier limits	hypothetical topography of the study area in the YD glacial phase
		reconstructed contour lines inside YD glacier limits	

The “Clip” tool was used with the original contour lines as input feature and the YD glacier limits as clip feature. The output feature contained the current topography in the YD glacier limits. This topography inside YD glacier limits was changed in order to estimate the topography of both YD and LIA glaciers. For this purpose, the “Editor” tool was used to modify every vertex of the original contour lines shapefile to a new position that represented the hypothetical volume of the glaciers. The TIN model from the new contour lines can be created to check if the paleo-topography is plausible, and to identify the areas which are not well defined. Once the paleo-topography inside the limits of YD glaciers is elaborated, the general model of the area was completed replacing the current contour lines by the new ones previously created. For this purpose, several tools were used. First, the tool “Erase” (ArcToolBox-Analysis Tools-Overlay-Erase) creates a feature maintaining only the portions of the input feature (original contour lines) falling outside the erase features (YD glacier limits). The output feature was a polyline shapefile of the study area without the contour lines inside YD glacier limits. To fill the empty parts, the tool “Merge” (ArcToolBox-Data Management Tools-General-Merge) was used to combine the erased contour lines of the study area (without the contour lines of YD limits) with the new hypothetical contour lines of the former glaciers previously created. The input features were the erased original contour lines and the new reconstructed contour lines inside YD limits; the output feature was the hypothetical topography of the study area in the YD glacial phase. Table 2.8 presents a summary of these steps.

The new contour lines need to be revised in order to confirm that all the vertexes in a same isoline are linked together. Occasionally, some vertexes appear separated and have to be snapped together using the “Snapping” tool in the “Editor” toolbar.

Once the reconstructed contour lines of former glaciers were obtained and revised, the contour belts both of the area and of each glacier have to be generated following steps 2 and 3 presented in table 2.2. First, with “Feature to Polygon” tool, the contour belts of the study area are created using as input features the new reconstructed topography and the polygon of the study area. Then, the contour belts of each glacier are generated using the “Clip” tool (Table 2.8).

Table 2. 7: Recall of the steps followed to obtain the contour belts of each glacier in the YD and LIA glacial phases.

Step	Tool	Input	Output
2	Feature to Plolygon	hypothetical topography of the study area in the YD glacial phase	contour belts of the study area
		polygon of the study area	
3	Clip	contour belts of the study area	contour belts of the selected glacier
		Clip feature: selected glacier polygon	

The result of step 2 is shown in figure 2.8 where the contour belts of figure 2.6 are compared to the modified ones. The result of step 3 is shown in figure 2.9 for glacier Hualcán1 in YD and LIA glacial phases. The procedure had to be repeated for each glacier for both LIA and YD glacier limits and the field “Area” was recalculated.

From this stage, ELA AABR calculations were completed in Microsoft Excel as explained in point 2.5.1. First, an Excel spread-sheet was completed for each glacier with the fields “ZInterval”, “Mean Z” and “Area m²” exported from the ArcMap10 attribute table. From this sheet the ELAs weighted by dfferent BR values were obtained and added to the second Excel spread-sheet to calculated de mean and standard deviation (see above 2.5.1).

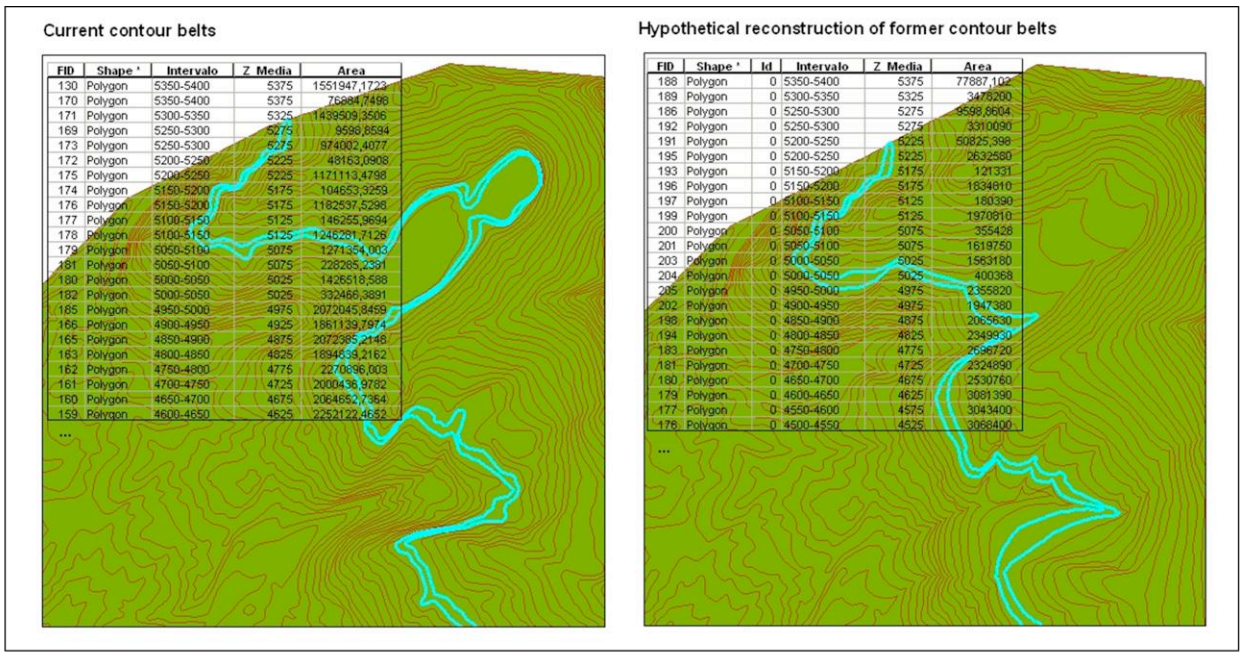

FID	Shape *	Intervalo	Z_Media	Area
130	Polygon	5350-5400	5375	1551947,1723
170	Polygon	5350-5400	5375	76864,7498
171	Polygon	5300-5350	5325	1439509,3506
169	Polygon	5250-5300	5275	9598,8594
173	Polygon	5250-5300	5275	974002,4077
172	Polygon	5200-5250	5225	48163,0908
175	Polygon	5200-5250	5225	1171113,4798
174	Polygon	5150-5200	5175	104653,3259
176	Polygon	5150-5200	5175	1182537,5298
177	Polygon	5100-5150	5125	146255,9694
178	Polygon	5100-5150	5125	1245281,7126
179	Polygon	5050-5100	5075	1271354,003
181	Polygon	5050-5100	5075	228285,2391
180	Polygon	5000-5050	5025	1426518,588
182	Polygon	5000-5050	5025	332466,3891
185	Polygon	4950-5000	4975	2072045,8459
166	Polygon	4900-4950	4925	1861139,7974
165	Polygon	4850-4900	4875	2072385,2148
163	Polygon	4800-4850	4825	1894839,2162
162	Polygon	4750-4800	4775	2270896,003
161	Polygon	4700-4750	4725	2000436,9782
160	Polygon	4650-4700	4675	2064652,7364
159	Polygon	4600-4650	4625	2252122,4652

FID	Shape *	Id	Intervalo	Z_Media	Area
188	Polygon	0	5350-5400	5375	77887,102
189	Polygon	0	5300-5350	5325	3478200
186	Polygon	0	5250-5300	5275	9598,8604
192	Polygon	0	5250-5300	5275	3310090
191	Polygon	0	5200-5250	5225	50825,398
195	Polygon	0	5200-5250	5225	2632580
193	Polygon	0	5150-5200	5175	121331
196	Polygon	0	5150-5200	5175	1834610
197	Polygon	0	5100-5150	5125	180390
199	Polygon	0	5100-5150	5125	1970810
200	Polygon	0	5050-5100	5075	355428
201	Polygon	0	5050-5100	5075	1619750
203	Polygon	0	5000-5050	5025	1563180
204	Polygon	0	5000-5050	5025	400368
205	Polygon	0	4950-5000	4975	2355820
202	Polygon	0	4900-4950	4975	1947380
198	Polygon	0	4850-4900	4875	2065830
194	Polygon	0	4800-4850	4825	2349930
183	Polygon	0	4750-4800	4775	2696720
181	Polygon	0	4700-4750	4725	2324890
180	Polygon	0	4650-4700	4675	2530760
179	Polygon	0	4600-4650	4625	3081390
177	Polygon	0	4550-4600	4575	3043400
176	Polygon	0	4500-4550	4525	3068400

Figure 2. 9: Comparison of current and former contour belts of the study area and a section of their respective attribute tables. Contour belt 4100-4150 is selected in both figures.

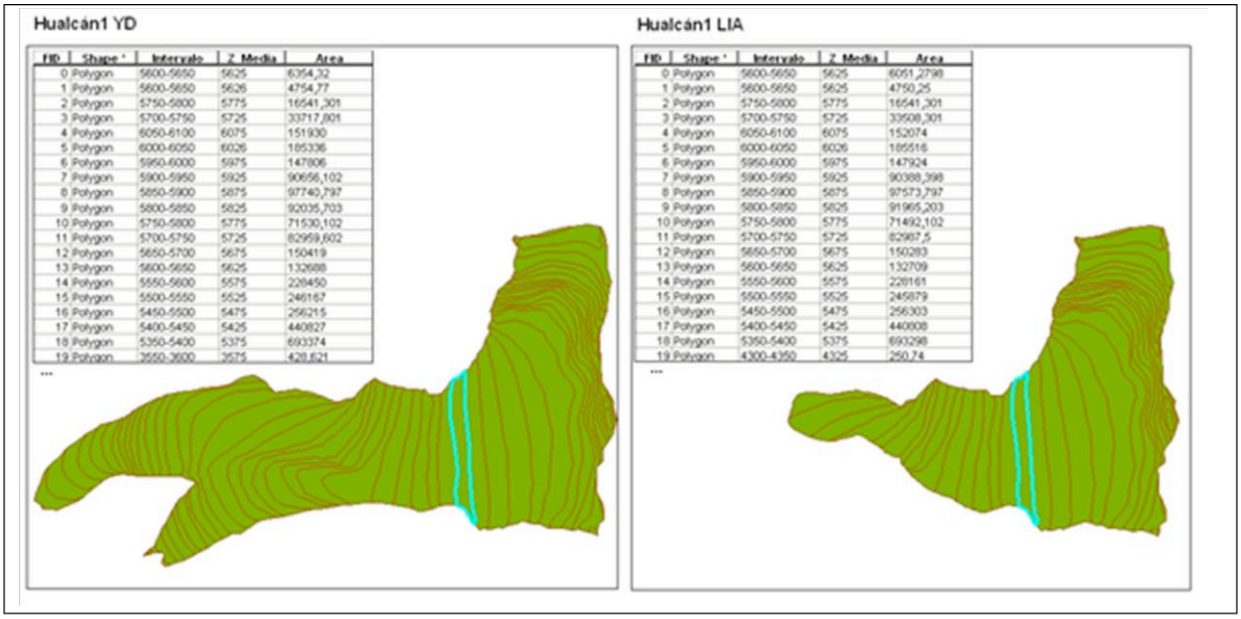

FID	Shape *	Intervalo	Z_Media	Area
0	Polygon	5600-5650	5625	6354,32
1	Polygon	5600-5650	5625	4754,77
2	Polygon	5750-5800	5775	16541,301
3	Polygon	5700-5750	5725	33717,801
4	Polygon	6050-6100	6075	151930
5	Polygon	6000-6050	6026	185336
6	Polygon	5950-6000	5975	147806
7	Polygon	5900-5950	5925	90656,102
8	Polygon	5850-5900	5875	97740,797
9	Polygon	5800-5850	5825	92035,703
10	Polygon	5750-5800	5775	71530,102
11	Polygon	5700-5750	5725	82959,602
12	Polygon	5650-5700	5675	150419
13	Polygon	5600-5650	5625	132688
14	Polygon	5550-5600	5575	228450
15	Polygon	5500-5550	5525	246167
16	Polygon	5450-5500	5475	256215
17	Polygon	5400-5450	5425	440827
18	Polygon	5350-5400	5375	693374
19	Polygon	3550-3600	3575	428,621

FID	Shape *	Intervalo	Z_Media	Area
0	Polygon	5600-5650	5625	6051,2798
1	Polygon	5600-5650	5625	4750,25
2	Polygon	5750-5800	5775	16541,301
3	Polygon	5700-5750	5725	33508,301
4	Polygon	6050-6100	6075	152074
5	Polygon	6000-6050	6026	185516
6	Polygon	5950-6000	5975	147924
7	Polygon	5900-5950	5925	90388,398
8	Polygon	5850-5900	5875	97573,797
9	Polygon	5800-5850	5825	91965,203
10	Polygon	5750-5800	5775	71492,102
11	Polygon	5700-5750	5725	82987,5
12	Polygon	5650-5700	5675	150283
13	Polygon	5600-5650	5625	132709
14	Polygon	5550-5600	5575	228161
15	Polygon	5500-5550	5525	245879
16	Polygon	5450-5500	5475	256303
17	Polygon	5400-5450	5425	440808
18	Polygon	5350-5400	5375	693298
19	Polygon	4300-4350	4325	250,74

Figure 2. 10: Example of contour belts and a section of their attribute tables for Hualcán1 in YD and LIA. Contour belt 5100-5150 is selected in both figures.

2.6 Spatial model of ELAs and accumulation and ablation zones

The results of the calculation of ELAs AABR offer five possible values of ELA both for each glacier and for the entire SW slope. They result from weighting the ELA by five different

BRs (see table 2.4). Osmaston´s step number 10 indicates to select the BR with the lowest standard deviation, which indicates the ELA with the best statistical probability of being correct. The principle is that: “a homogeneous group of glaciers (i.e. of similar type in an environmentally homogeneous restricted area) should react similarly to the climate they experience. Hence their ELAs should be closely similar, differentiated only by such local individual factors as shading by valley-side precipices. In statistical terms the standard deviation of these individual ELAs from the group mean value will be less than that of other possible sets of ELA estimates from their means. Therefore, for each input value of the ratio we should calculate the standard deviation of its predictions (or the standard error of the mean), and select the value which has the smallest standard deviation” (Osmaston, 2005). Following this indication, the most representative value of ELA for the group of glaciers on the SW slope of Nevado Hualcán was that of the general SW slope which has the smallest standard deviation (blue in table 2.4).

2.6.1 ELAs spatial model

The altitude of ELA on the SW slope of Nevado Hulacán in the four different glacial phases can be marked in a map using ArcMap10.

Table 2. 8: Summary of the steps followed to obtain the ELAs spatial model

Step	Tool	Input	Output
1	Dissolve	glacier limits	outermost glacier limits
2	Create TIN	contour lines of the study area	TIN
3	Surface Contour	TIN	1 m contour lines
4	Intersect	outermost glacier limits	ELA spatial model
		selected 1 m contour line representing the ELA	

The ELAs to be represented are those of the overall SW slope. Hence, it was necessary to create a unique polygon comprising the outermost limits of glaciers in each glacial phase. This was done with the “Dissolve” tool (ArcToolBox-Data Management Tools–Generalization–Dissolve) using the original glacier delimitation layers as input (point 2.4).

The altitudes of ELAs are at the level of significance of meters. The contour lines used so far have a 50 m vertical interval. Therefore, a 1 m vertical interval contour line layer had to be generated. This was done by creating a TIN model of the study area from the 50 m resolution contour lines and, from which, the 1 m resolution contour lines were generated. The tool “Create TIN” (ArcToolBox-3D Analyst Tools-TIN Management-Crete TIN) creates a TIN model from a given spatial reference layer which contains a “height-field”. In this case, two different TIN models were created. The first used the original 50 m resolution contour line layer of the study area as the height reference. The second used the

reconstructed 50 m resolution contour line layer of the study area (point 2.5.2). Then, the "Surface contour" tool (ArcToolBox-3D Analyst Tools-Terrain and TIN Surface–Surface Contour) allowed creating a 1 m resolution contour line layer from each TIN model.

Finally, to map the corresponding ELAs in each glacial phase, the "Intersect" tool was applied taking as input features the outermost limit of glaciers and the selected contour line representing the ELA in the designated glacial phase. "Select by attributes" tool from the attribute table was used to select the precise contour line. This procedure was repeated for every glacial phases. Note that for 2003 and 1962, the 1 m resolution contour lines used were the ones derived from the original 50 m resolution topography. For LIA and YD the contour lines were the ones derived from the reconstruction of the paleo-topography. Table 2.7 summarizes this procedure.

2.6.2 Accumulation and ablation zones spatial model and surface calculation

The first definition of ELA presented at the beginning of point 2.5 was that it is the theoretical line dividing the accumulation zone and the ablation zone. This definition lays the foundations of this phase. If the polygons representing the outermost limits of glaciers are divided in two different polygons cut through their respective ELAs, the accumulation and ablation zones´ surfaces can be inferred.

In order to section a polygon through a line the following steps needed to be carried out (Table 2.10).

Table 2. 9: Summary of the steps followed to obtain the accumulation and ablation zone´s spatial model.

Step	Tool	Input	Output
1	Polygon to line	outermost glacier limits	outermost glacier limits as polyline
2	Editor	cut glacier polylines over the intersection with ELA	
3	Merge	cut glacier polylines over the intersection with ELA	single polyline layer
		ELA	
4	Feature to polygon	single polyline layer with acc/abl selected lines	acc/abl zones spatial model

Step 1 uses "Polygon to Line" tool (ArcToolBox-Data management Tools–Features–Polygon to Line) to transform the polygon representing the outermost limits of glaciers into a polyline feature. The "Split tool" from the "Editor" toolbar allowed cutting the newly created polylines where they intersected with the ELA polyline. Then, the "Merge" tool was used to combine the polylines from both the glacier limits and the ELA shapefiles into one single polyline shapefile. From this single shapefile, the polylines delimiting the

accumulation zone were selected and served as input for the “Feature to Polygon” tool to create a polygon from the selected lines. The same procedure was followed to create the ablation zone. The entire process had to be repeated for each glacial phase. New single polygons and their respective attribute tables were generated for each accumulation and ablation zones in every glacial phase.

To calculate the surfaces of accumulation and ablation zones, a new field was added in each attribute table called “Areakm2”. Surfaces were calculated with the “Calculate Geometry” tool form the attribute table. The unit used was km².

ANNEX: Number of the aerial photographs used in this work.

NUMBER	DATE
41094	23 May 1963
41093	23 May 1963
41092	23 May 1963
19774	5 July 1962
19773	5 July 1962
19772	5 July 1962
16725	19 June 1962
16724	19 June 1962
16723	19 June 1962
16531	19 June 1962
16533	19 June 1962
16532	19 June 1962
14234	15 June 1962
14233	15 June 1962
14232	15 June 1962

CHAPTER 3

RESULTS

Tropical glaciers are a high-confident climate indicator and a valuable element in early detection strategies (WGMS, 2008). The purpose of this work was to delimit glaciers on the SW slope of Nevado Hualcán in four different glacial phases through moraine mapping and photointerpretation, and to calculate their surfaces and ELAs in order to achieve quantitative information for further studies. Glacier surface retreat and ELA vertical shift are indirect responses to climate change, and therefore so called indirect methods of describing glacier fluctuations (see chapter 2). The results that follow describe first the cartography of the moraines, secondly the delimitation and surface calculation of glaciers and finally the estimation of ELAs AABR and the accumulation and ablation zones.

3.1 Moraine mapping

Moraines are a recognizable geomorphological evidence of the traces left behind by glaciers, and they serve as reference for paleo-glacier reconstruction. The relative dating of the moraines mapped in the SW slope of Nevado Hualcán was based on chronologies previously published and summarized in Table 3.1.

Table 3. 1: Relative dating classification of moraines.

Period	Relative dating	Reference publications
preLLGM	440 - 65 ka BP	Farber et al. (2005) Smith et al. (2005)
LLGM	34 - 21 ka BP	
postLLGM	20 - 16 ka BP	
YD	12,5/12,4 ka BP	Glasser et al. (2009)
postYD	11,3-10,7; 9,7; 7,6 ka BP	
LIA	1590 - 1720	Solomina et al. (2007)
XXth century	1920s and 1970s	Kaser (1999)

The resulting moraine cartography over the SPOT image is presented in Fig. 3.1. As shown, single moraines were identified and color-coded for each relative dating. The youngest moraines were formed during the XXth century advances which occurred mainly in 1920s and 1970s (Kaser, 1999). These moraines were found between 4070 and 4900 m. The youngest main glacier advance occurred during the Little Ice Age (LIA) between 1590 and 1720 (Solomina et al., 2007), and left prominent fresh moraines between 4050 and 4800 m. The lakes Checquiacocha, Rajupaquinan, Cochca and 513 are dammed by LIA moraines. The next previous marked advance took place during the Younger Dryas Chronozone (YD), around 12,5-12,4 ka BP (Glasser et al., 2009). This advance left prominent moraines down-valley from LIA, between 3460 and 4480 m. Inside these large YD lateral moraines, between YD and LIA, smaller moraine systems are found from later stillstands or minor advances dated to 11.3–10.7, 9.7 and 7.6 ka BP (Glasser et al., 2009).

The Local Last Glacial Maximum (LLGM) moraines are the most prominent ones down-valley from the YD and were found between 3350 and 4080 m. They may have been deposited between 34 ka and 21 ka BP, earlier then the global LGM commonly defined at 21 ka BP. Flanked by LLGM and YD moraines, there were smaller moraines formed during the still/readvances between 20 and 16 ka BP between 3460 and 4070 m. Finally, the oldest moraines, between 3000 and 3500 m, testify that larger glaciations preceded LLGM. Moraines appearing as “Unclassified” belong to a section of the study area where mass movements and landslides have altered the valley´s morphology and need a more complex geomorphological interpretation by means of landform identification and absolute dating studies.

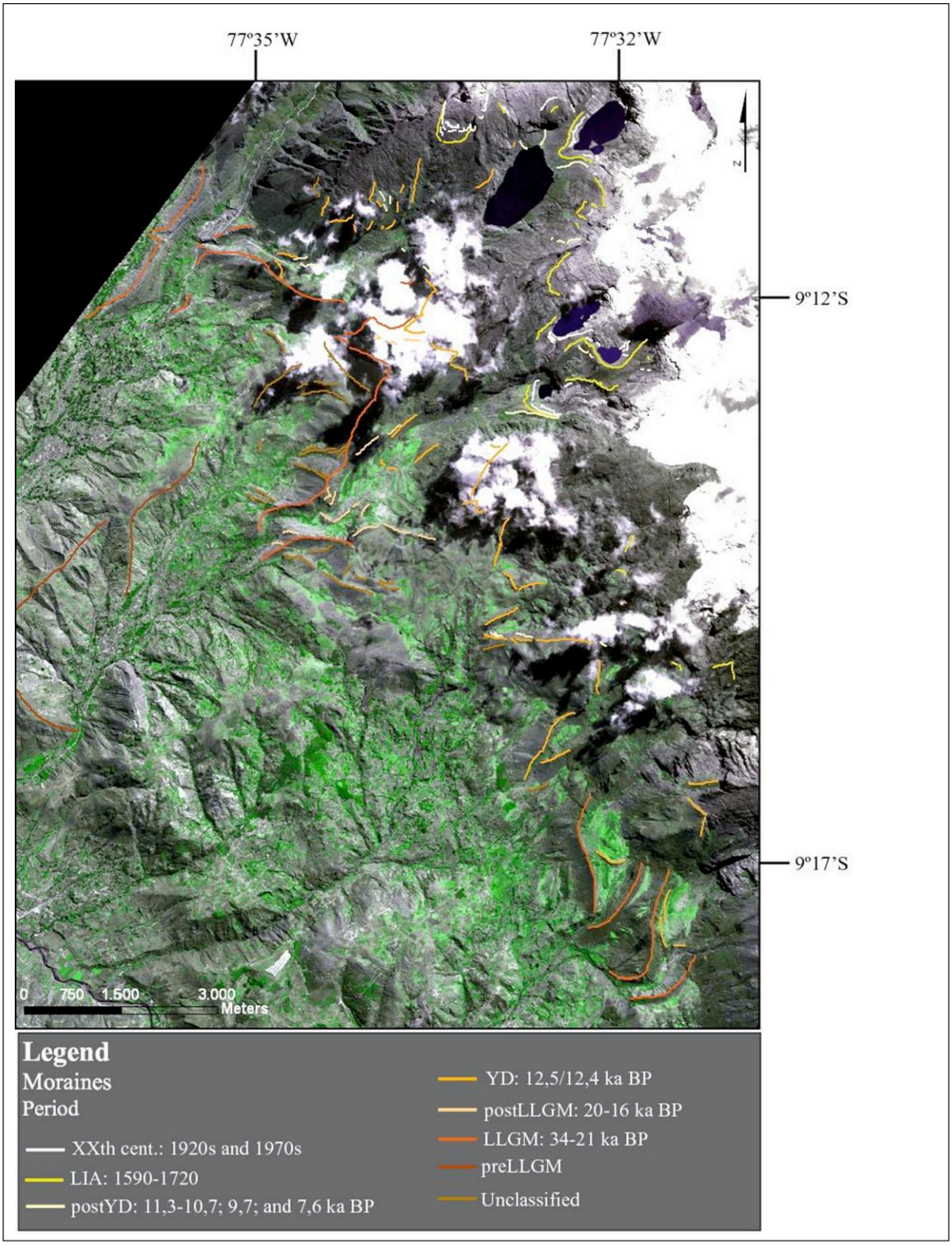

Figure 3. 1: Moraine mapping over SPOT image. Moraines are classified by their relative dating.

3.2 Glacier delimitation and surface calculation

The delimitation of glaciers on the SW slope of Nevado Hualcán was established for four glacial phases: 2003, 1962, LIA and YD from which their surfaces were inferred. This provided quantitative information of glacier evolution for future climatic analysis.

Figures 3.2 and 3.3 show the delimitation of the SW facing glaciers in the four glacial phases and the calculation of their total surface. The reference materials to delimit glaciers in 2003 and 1962 were the Google Earth images and the aerial photographs (1962 flight) respectively. The reference material to delimit LIA and YD glaciers was the moraine mapping. Glacier Alancay in 1962 was drawn with dashed lines and its surface values indicated in italics. Its limits and surface values were approximated because the aerial photographs did not cover this area (see part 2.4).

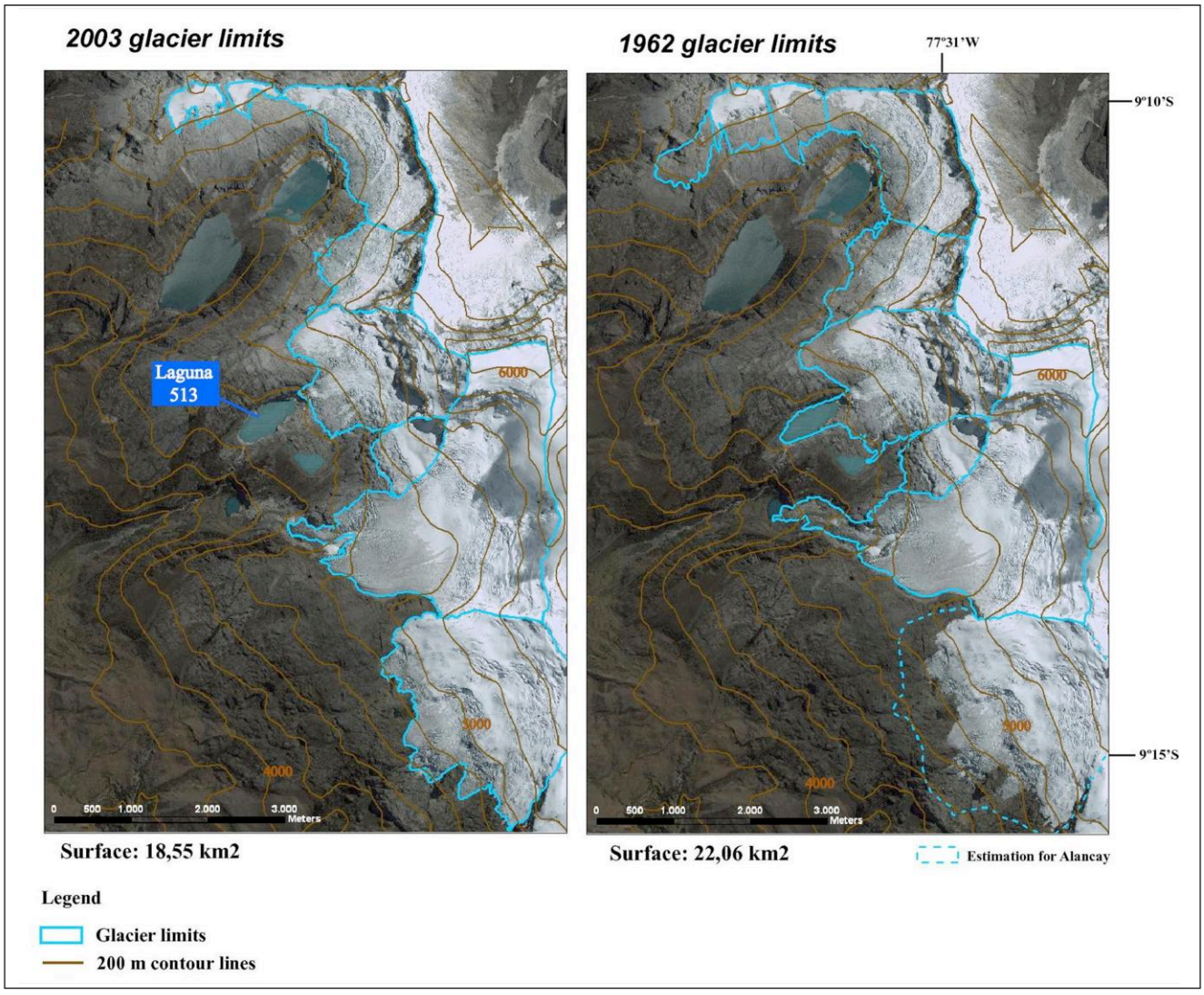

Figure 3. 2: Glacier delimitation in 2003 and 1962. Laguna 513 is formed by mid-1980s.

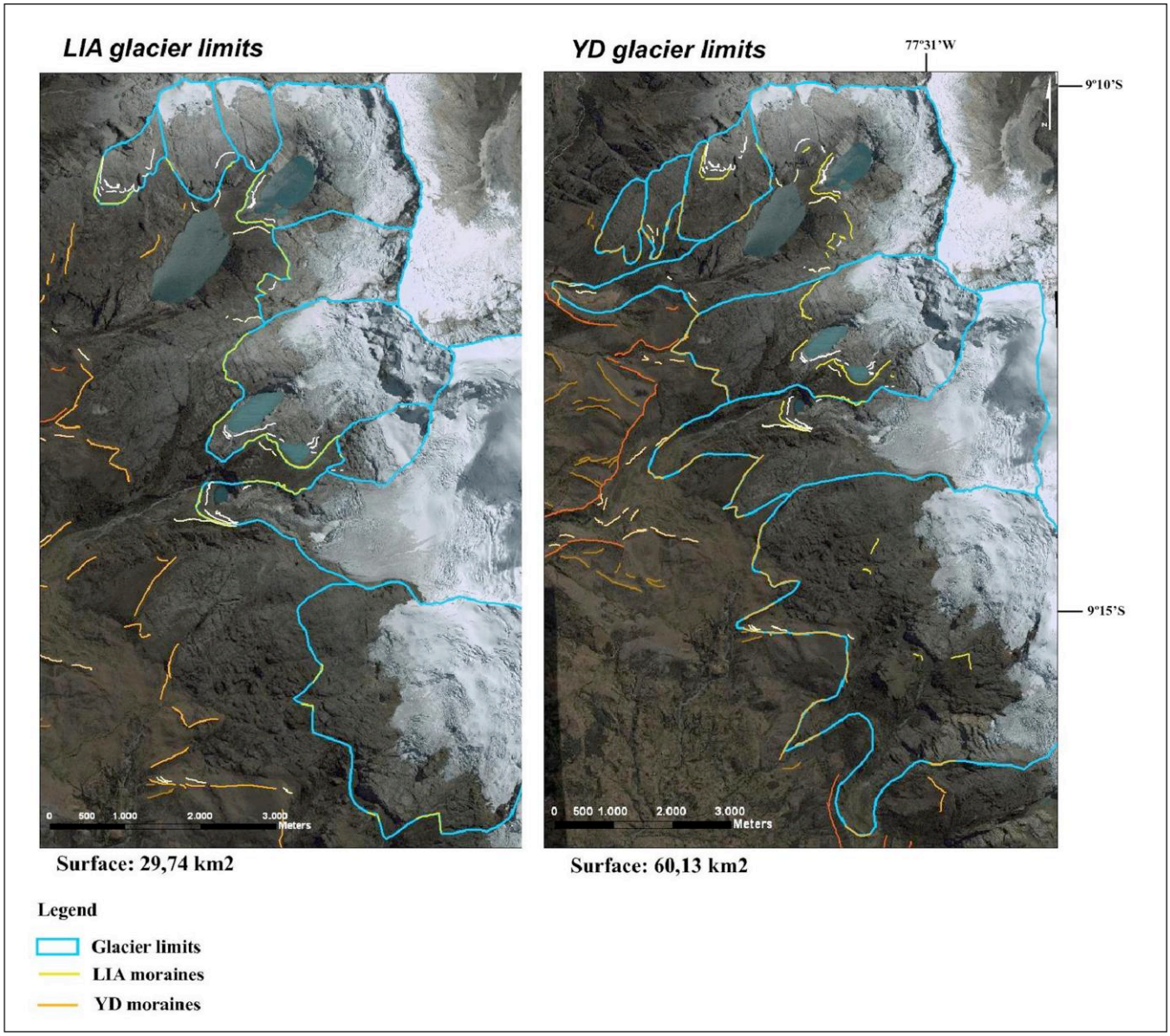

Figure 3. 3: Glacier delimitation in LIA and YD.

In 2003 glaciers extended from the upper limits above 5000 m for Gatay2 and 6000 m for Hualcán1, to the terminus above 4600 m and 4300 m respectively. Glaciers in 2003 had areas from 6,54 km² (Hualcán1) to 0,29 km² (Gatay4) (Table 3.2). The results show that the surface of glaciers has retreated 41,6 km² from YD to 2003. Glacier surface in 2003 was 30,9% of the surface of glaciers in YD. Around three to four centuries ago, during the LIA period, glacier surface was 11,18 km² larger than in 2003. This indicates that these glaciers were 37,6% larger than today (Fig. 3.5). From 1962 to 2003 glacier surface retreated 3,1 km², which corresponds to a deglaciation rate of 0,076 km²/year (76.000 m²/year). If the value 1655 is taken as the mean date for the LIA period, the surface retreat rate between LIA and 1962 was 0,025 km²/year. This shows that glacier retreat has accelerated during the XXth century. By mid-1980s Laguna 513 formed (Carey 2010, see Fig 3.2).

The total glaciated surface of the SW slope of Nevado Hualcán in each glacial phase is presented in Figs. 3.4 and 3.5. As shown, the total surface of the group of glaciers decreases along the period studied. Compared to YD, the total surface of the following glacial phases represents a decreasing percentage: LIA´s glaciated surface was 49,5% of the surface in YD, retreating 30,4 km²; 1962 represents 36,7% of the YD, and only 30,9% of the YD glaciated surface remains by 2003, with a retreat of 41,6 km². Note that in Fig. 3.4 the scale in abscissa is not linear and the rate of glacier surface decrease actually increases along time.

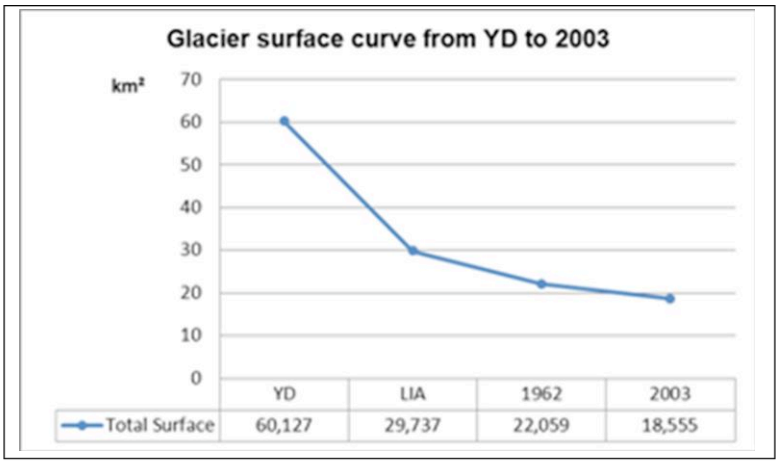

Figure 3. 4: Total glaciated area on the SW slope of Nevado Hualcán in the four glacial phases.

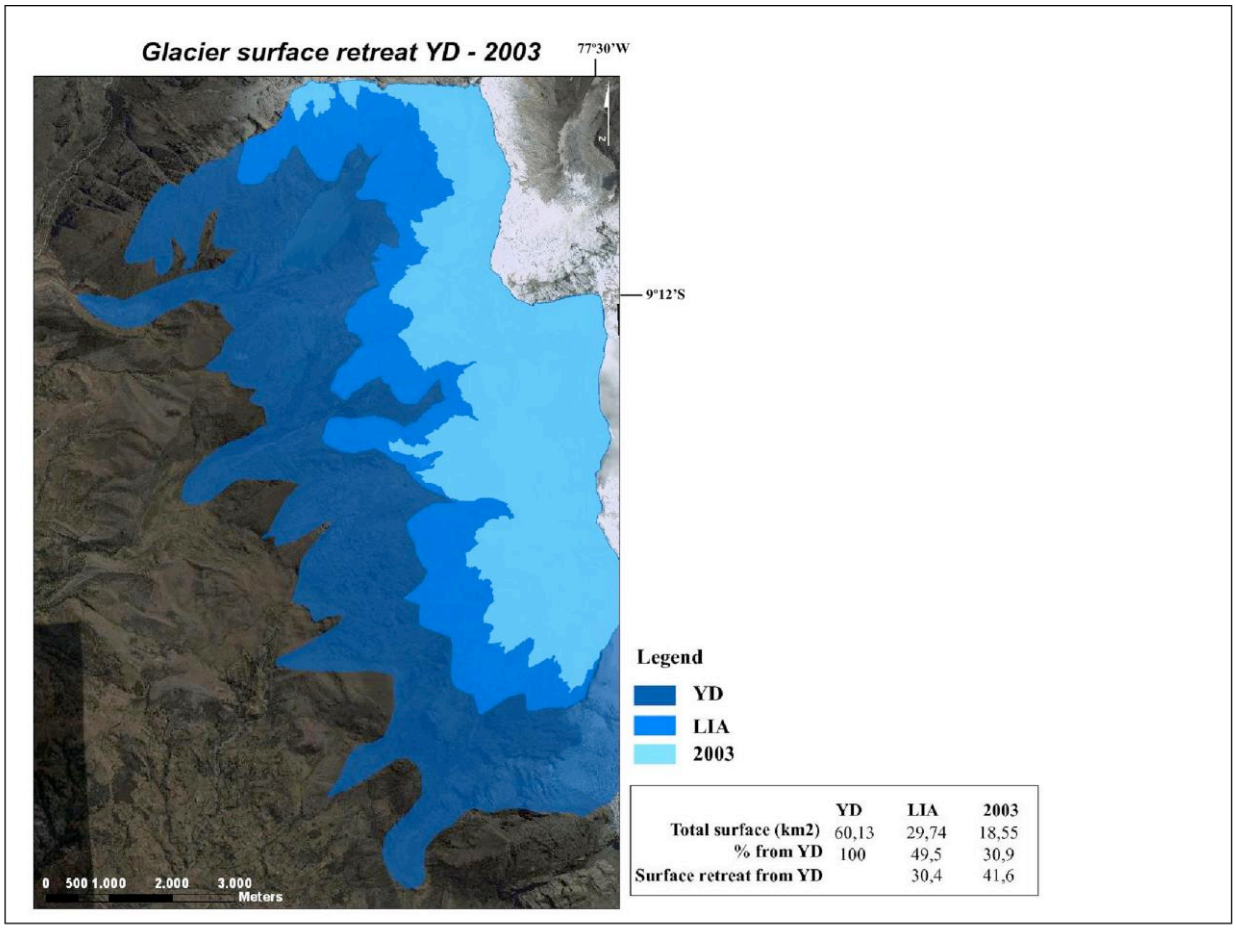

Figure 3. 5: Glacier surface retreat from YD to 2003.

Surface curves for glaciers Hualcán 1 and 3 are displayed in Fig. 3.3 as an example of the general trend of glaciers´ surface curves on the study area (see Fig. 2.6 in chapter 2 for the names given to glaciers). The surfaces of each glacier in every glacial phase are brought together in table 3.2. The surface of single glaciers also show a decrease along the period studied, and some glaciers, such as Gatay 5, 6 and 7, even disappear.

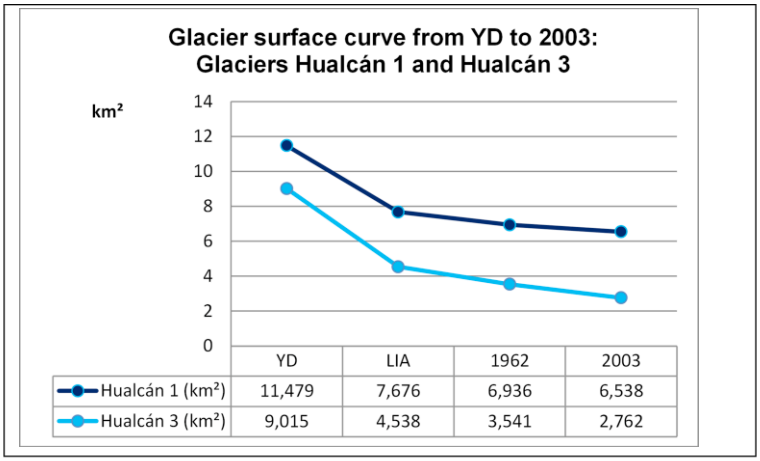

Figure 3. 6: Surface curve of glaciers Hualcán 1 and 3 in the four glacial phases.

In summary, it was possible to map the limits and surface of current and former glaciers from aerial photographs, high resolution images and moraines, and this allowed reconstructing the evolution of the areas of these glaciers.

Table 3. 2: Glacier surfaces in the four studied glacial phases and the percentage they represent respect to the YD phase.

Glacier	Surfaces (km²)			
	YD	LIA	1962	2003
Alancay	23,644	8,736	*5,226*	4,836
Hualcán 1	11,479	7,676	6,936	6,538
Hualcán 2	9,015	0,929	0,843	0,626
Hualcán 3		4,538	3,541	2,762
Gatay 1	12,323	1,953	1,677	1,274
Gatay 2		3,430	2,368	2,071
Gatay 3		0,740	0,548	0,156
Gatay 4		1,111	0,550	0,291
Gatay 5	2,166	0,624	0,370	0
Gatay 6	0,768	0	0	0
Gatay 7	0,731	0	0	0
TOTAL	**60,127**	**29,737**	***22,059***	**18,555**
%	**100**	**49,5**	***36,7***	**30,9**

3.3 ELAs AABR

The difference in altitude between modern and former ELAs has been widely used to estimate climate change (Benn et al. 2005). The method of ELAs AABR for glacier reconstruction requires knowledge on the limits of glaciers and of the area and mean altitude of the contour belts that fall inside each glacier limit. This information allows calculating the ELAs AABR using Osmaston´s Excel spread-sheet. In the case of paleo-glaciers, the topography had to be reconstructed in order to estimate the ice surface and volume. The result of the paleo-topography reconstruction of the YD glacial phase on the SW slope of Nevado Hualcán is shown in Fig. 3.7.

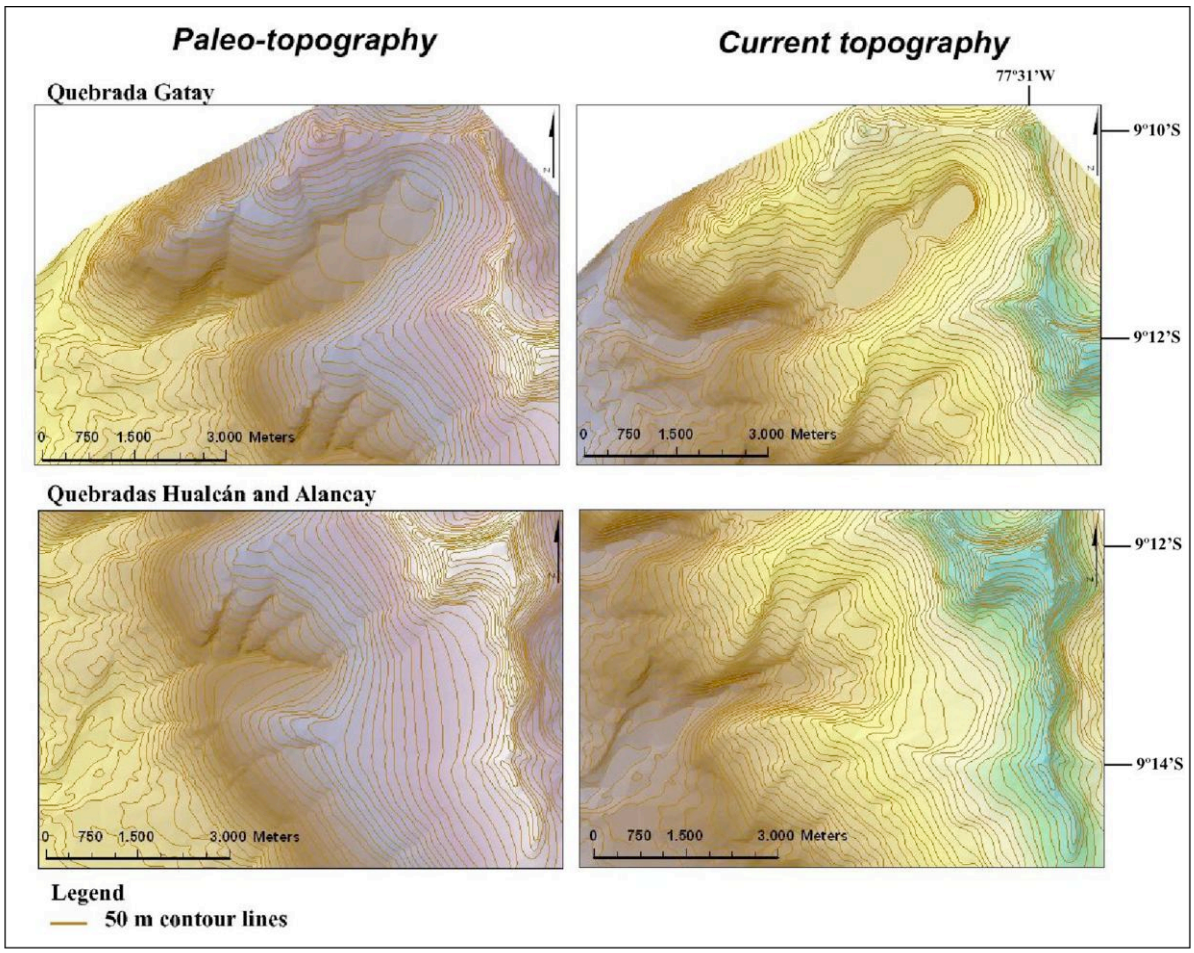

Figure 3. 7: Paleo-topography reconstruction.

Osmaston´s Excel spread-sheets calculate first the ELA AA (Area x Altitude method) following Sisson´s equation, which then is weighted by different values of BR. The BR with the lowest standard deviation indicates the ELA with the best statistical probability of being correct and was selected as the most representative ELA value for the group of glaciers (see part 2.5 in chapter 2). Tables 3.3 to 3.6 present the resulting summary tables of ELA AABR calculations for each glacial phase. The most representative ELA AABR values for

the SW slope of Nevado Hualcán in each glacial phase are highlighted in blue and were plotted on a map (Figs. 3.10 and 3.11).

Table 3. 4: Summary table of ELAs AABR in 2003

SW slope Nevado Hualcán: ELAs AABR 2003

	ELA SW slope	**5124**	**(BR=1)**		
	ELA Quebrada Hualcán	5196	(BR=1,5)		
	ELA Quebrada Gatay	5074	(BR=1,5)		
QUEBRADA HUALCÁN	BR=1	**BR=1,5**	BR=2	BR=2,5	BR=3
Hulacán 1	5283	5275	5315	5343	5363
Hualcán 2	5108	5112	5126	5135	5142
Hualcán 3	5152	5200	5233	5255	5272
Mean	5181	**5196**	5225	5244	5259
Standard deviation	91	**82**	95	104	111
QUEBRADA GATAY	**BR=1**	BR=1,5	BR=2	BR=2,5	BR=3
Gatay 1	5174	5159	5181	5197	5208
Gatay 2	4989	4962	4955	4968	4977
Gatay 3	5024	5015	5009	5005	5002
Gatay 4	5110	5102	5110	5115	5119
Mean	**5074**	5060	5064	5071	5077
Standard deviation	**84**	88	101	105	107
QUEBRADA ALANCAY	BR=1	BR=1,5	BR=2	BR=2,5	BR=3
	5150	5188	5213	5231	5244
SW SLOPE	**BR=1**	BR=1,5	BR=2,0	BR=2,5	BR=3
Mean	**5124**	5127	5143	5156	5166
Standard deviation	**90**	102	119	127	133

Table 3. 3: Summary table of ELAs AABR in 1962

SW slope Nevado Hualcán: ELAs AABR 1962

	ELA SW slope	**5018**	**(BR=1,5)**		
	ELA Quebrada Hualcán	5104	(BR=1,5)		
	ELA Quebrada Gatay	4967	(BR=1,5)		
QUEBRADA HUALCÁN	BR=1	**BR=1,5**	BR=2	BR=2,5	BR=3
Hulacán 1	5235	5230	5274	5306	5329
Hualcán 2	5059	5068	5086	5098	5107
Hualcán 3	5041	5015	5052	5078	5097
Mean	5112	**5104**	5137	5161	5178
Standard deviation	107	**112**	120	126	131
QUEBRADA GATAY	BR=1	**BR=1,5**	BR=2	BR=2,5	BR=3
Gatay 1	5091	5052	5072	5089	5102
Gatay 2	4959	4968	4986	4998	5007
Gatay 3	4904	4902	4901	4901	4901
Gatay 4	5028	5008	5005	5015	5022
Gatay 5	4911	4904	4914	4921	4926
Mean	4979	**4967**	4976	4985	4992
Standard deviation	80	**65**	70	76	80
SW SLOPE	BR=1	**BR=1,5**	BR=2	BR=2,5	BR=3
Mean	5029	**5018**	5036	5051	5061
Standard deviation	108	**105**	118	127	134

Table 3. 5: Summary table of paleoELAs AABR in LIA

SW slope Nevado Hualcán: ELAs AABR Little Ice Age

	paleoELA SW slope	**4994**	**(BR=1)**		
	paleoELA Quebrada Hualcán	5101	(BR=1,5)		
	paleoELA Quebrada Gatay	4921	(BR=1)		
QUEBRADA HUALCÁN	BR=1	**BR=1,5**	BR=2	BR=2,5	BR=3
Hualcán 1	5242	5223	5269	5303	5330
Hualcán 2	5081	5052	5067	5081	5092
Hualcán 3	5026	5028	5063	5087	5105
Mean	5116	**5101**	5133	5157	5176
Standard deviation	112	**106**	118	126	134
QUEBRADA GATAY	**BR=1**	BR=1,5	BR=2	BR=2,5	BR=3
Gatay 1	5067	5072	5097	5115	5128
Gatay 2	4883	4854	4880	4898	4911
Gatay 3	4877	4850	4868	4881	4891
Gatay 4	4907	4924	4945	4960	4971
Gatay 5	4873	4853	4858	4867	4873
Mean	**4921**	4911	4930	4944	4955
Standard deviation	**82**	95	100	102	104
QUEBRADA ALANCAY	**BR=1**	BR=1,5	BR=2	BR=2,5	BR=3
	4994	4959	4997	5024	5044
SECTOR SW	**BR=1**	BR=1,5	BR=2	BR=2,5	BR=3
Mean	**4994**	4979	5005	5024	5038
Standard deviation	**124**	126	135	141	146

Table 3. 6: Summary table of paleoELAs AABR in YD

SW slope Nevado Hualcán: ELAs AABR Younger Dryas

	paleoELA SW slope	**4652**	**(BR=1)**		
	paleoELA Quebrada Hualcán	4874	(BR=1)		
	paleoELA Quebrada Gatay	4537	(BR=1)		
QUEBRADA HUALCÁN	**BR=1**	BR=1,5	BR=2	BR=2,5	BR=3
Hualcán 1	4934	4965	5033	5083	5120
Hualcán 23	4814	4417	4696	4714	4721
promedio	**4874**	4691	4865	4899	4921
desviación típica	**85**	387	238	261	282
QUEBRADA GATAY	**BR=1**	BR=1,5	BR=2	BR=2,5	BR=3
Gatay 1234	4688	4674	4717	4748	4772
Gatay 5	4637	4602	4620	4638	4651
Gatay 6	4493	4459	4464	4482	4495
Gatay 7	4330	4302	4324	4340	4352
promedio	**4537**	4509	4531	4552	4568
desviación típica	**161**	165	173	179	183
QUEBRADA ALANCAY	BR=1	BR=1,5	BR=2	BR=2,5	BR=3
Alancay	4666	4531	4572	4579	4582
SW SLOPE	**BR=1**	BR=1,5	BR=2	BR=2,5	BR=3
promedio	**4652**	4564	4632	4655	4670
desviación típica	**199**	215	223	235	243

Values of ELAs and paleoELAs AABR allow the analysis of their vertical shift from YD to 2003. Figure 3.8 shows the altitude values of ELA AABR in the four glacial phases and Fig. 3.9 presents the vertical shift in ELAs (ΔELA). The altitude of ELA AABR has shifted 472 m from YD to 2003. Between 1962 and 2003, the shift was of 106 m, which indicates a vertical shift of 2,59 m/year; compared to the vertical shift rate between LIA and 1962, take 1655 as the men date for LIA, the shift in this previous period was 0,08 m/year. This result illustrates the accelerating rate of shift during the XXth century. As before, note that in Fig. 3.8 and 3.8, the scale in abscissa is not linear and the rate of chage of ELA and ELA shifts actually increase with time.

In summary, the results of ELA AABR show that the ELA vertical shift was 472 m from YD, 130 m from LIA and 106 m from 1962. Changes in ELA are caused by changes in climatic conditions (temperature, precipitation, humidity and/or effective global radiation), hence the study of ELAs offer valuable quantitative information to analyze climatic forcing.

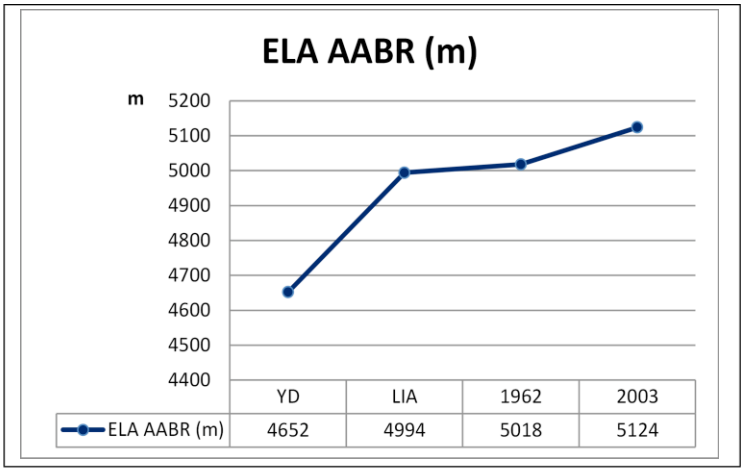

Figure 3. 8: ELAs AABR curve of the SW slope of Nevado Hualcán in four glacial phases.

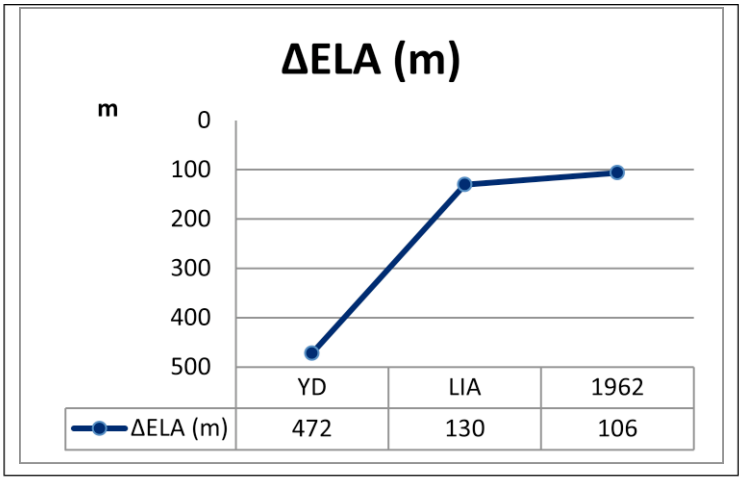

Figure 3. 9: Vertical shift in ELAs AABR (ΔELA) respect to 2003.

3.4 Spatial model of ELAs and accumulation and ablation zones

ELAs represent the imaginary line dividing the accumulation and the ablation zones. As ELAs shift to higher altitudes, the accumulation zones of glaciers get smaller. When the ELA altitude shifts above the upper limit of a glacier, its accumulation zone disappears, and also its positive mass balance. In these conditions, the glacier is in a terminal phase and will eventually disappear in the time needed by the environmental conditions to melt the remaining ice. Hence, ELAs can be used as an indicator to predict future disappearance of glaciers.ELAs AABR for each glacial phase were plotted over the Google Earth images and presented in Figs. 3.10 and 3.11. During the YD glacial phase, the ELA AABR was above glacier Gatay7 and very close to the upper limit of glacier

Gatay6. The result of this can be seen in the LIA phase, where these glaciers have disappeared. The same behavior was observed in glacier Gatay5 from 1962 to 2003. In 2003, the altitude of ELA AABR can be compared to the upper limits of glaciers. Glaciers Gatay3 and a part of Gatay2 are below the ELA AABR which means that they will eventually disappear. Glacier Gatay2´s highest altitude is 5512 m (Nevado Cancará), 388 m above the ELA value, and glacier Gatay4´s highest altitude is 5286 m (Nevado Checquiacraju), just 162 m above the ELA. If, as indicated in part 3.3 the ELA shifts 2,59 m/year, and assuming that this rate remains constant, Glacier Gatay4 will be below the ELA in less than 63 years, and Glacier Gatay2 in less than 150 years. This first approximation to a future scenario of glacier retreat based on the ELA vertical shift, shows that the altitude of ELA can be taken as an indicator to predict future evolution of glaciers.

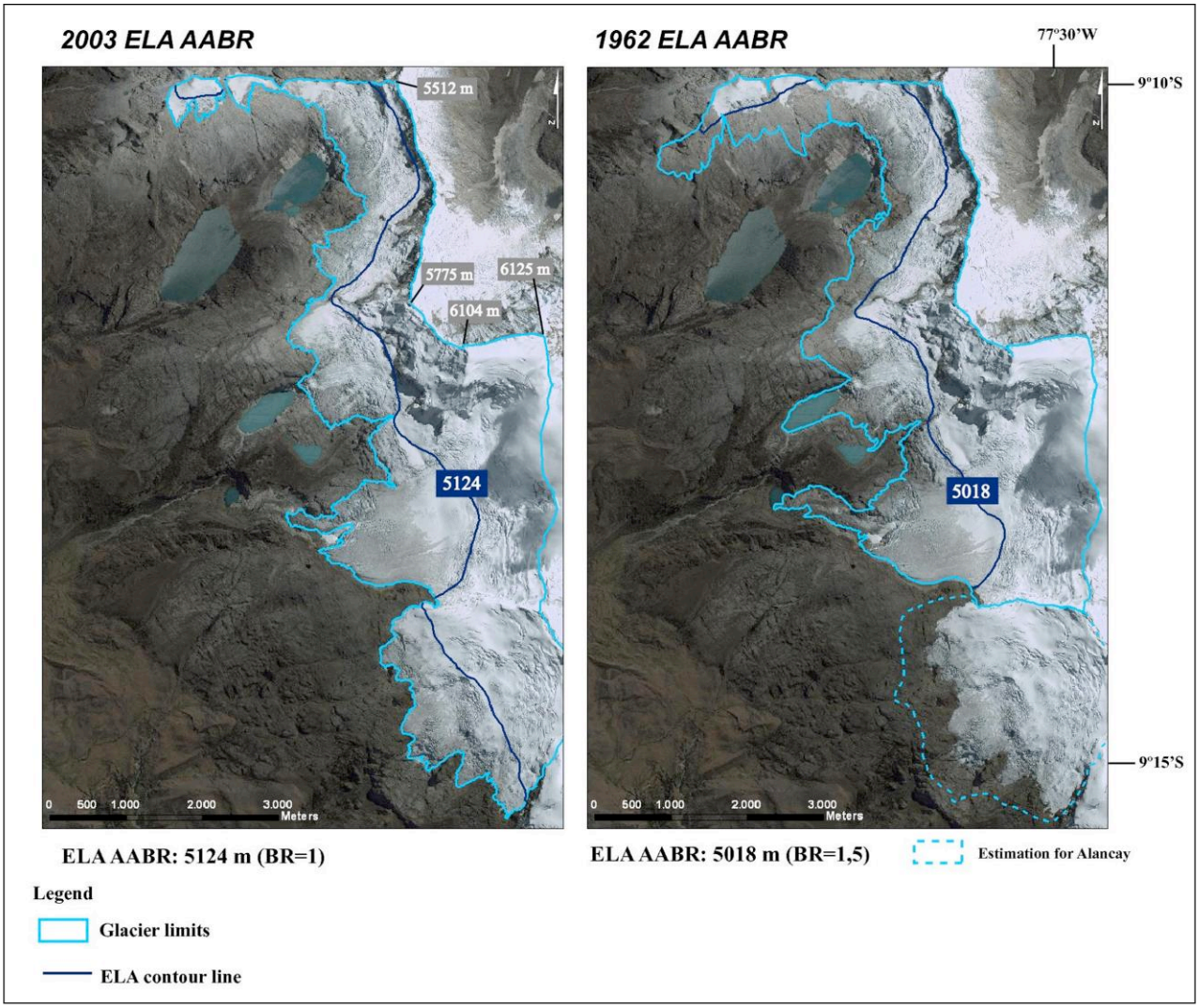

Figure 3. 10: Altitude of ELAs AABR for 2003 and 1962

As mentioned above, changes in ELAs are caused by changes in climatic conditions, thus climatic interpretations may be studied based on ELAs vertical shifts. Úbeda (2010) uses

an equation which assumes that the changes in ELA (ΔELA) are entirely a function of the changes in temperature (ΔT). The equation calculates the temperature shift from the product of the Moist Adiabatic Lapse Rate (MALR) and the shift in ELA (ΔELA):

$$\Delta T = \text{MALR x } \Delta ELA.$$

This equation offers a first approximation to further analysis on climatic forcing. The ΔELA chosen here was that of LIA with respect to 2003 (Fig. 3.9), which is 130 m. The MALR used was 6ºC/km (0,006 ºC/m), according to Smith et al. (2005) and Klein et al (1999). MALR varies according to how much moist is contained in the air. Further studies need to be undertaken in order to establish the specific MALR of the SW slope of Nevado Hualcán through climatic information. The application of the equation gives a temperature shift of 0,78 ºC from LIA to 2003. Shift in ELAs may be used to estimate climate change, but local factors such as complex topography (shading by steep valley walls, debris, orographic precipitation) have to be considered as they could mislead in the accuracy of the results

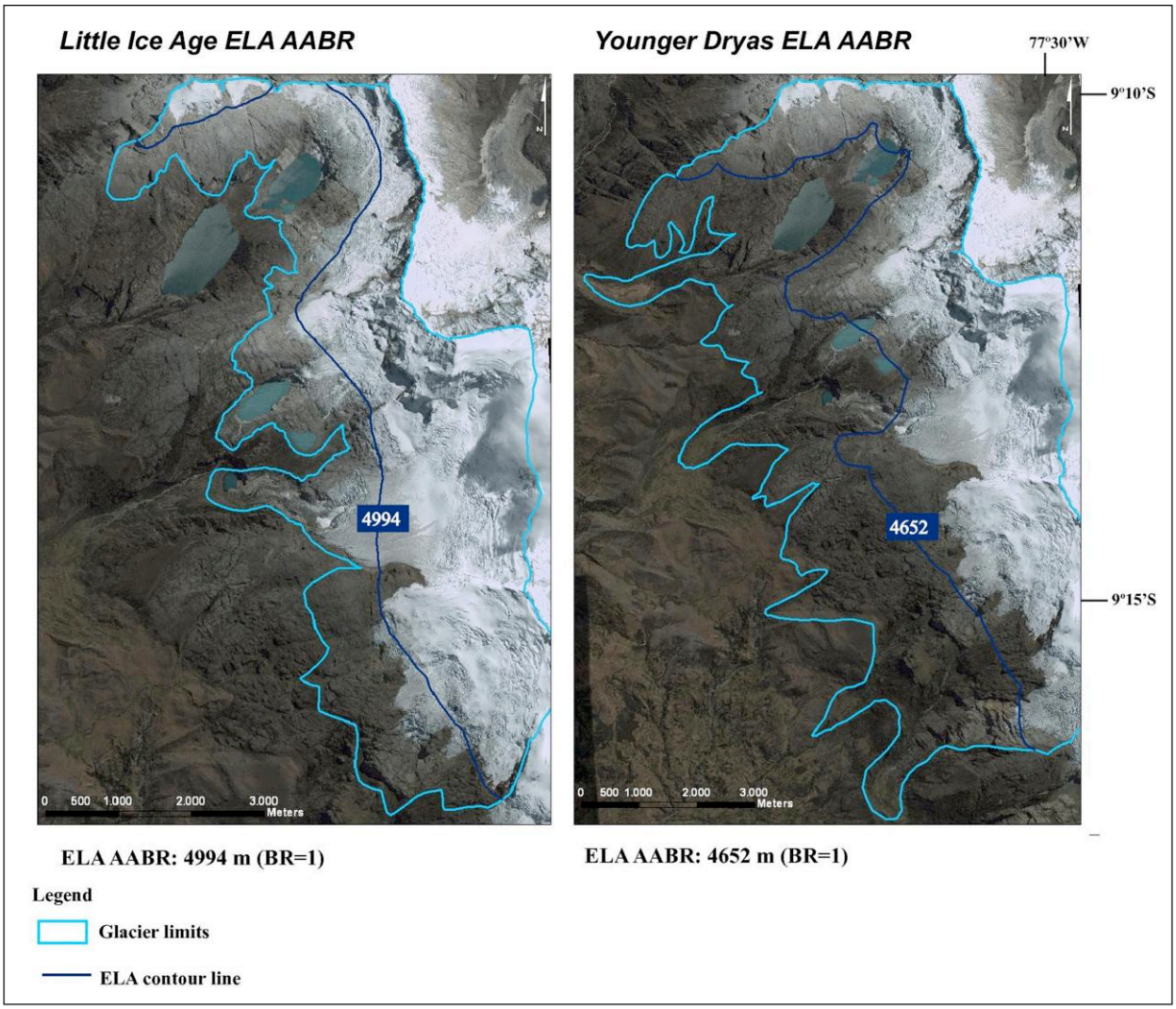

Figure 3. 10: Altitude of ELAs AABR for LIA and YD

obtained.

The reduction of the surface of the accumulation zone, caused by the shift of the ELA altitude, leads to a decrease of the ablation zone which results in the retreat of the entire glacier. Table 3.7 and Fig. 3.11 show the surface of the accumulation and ablation zones and their percentage with respect to the total surface of the glaciers. The area of the accumulation zone decreased 23,2 km² from YD to 2003, and the ablation zone decreased 18,3 km². This explains that the percentage of the accumulation zones over the total surface of the glaciers remain quite stable over the studied period, being 54,4% in YD and 51% in 2003. The Accumulation Area Ratio (AAR) is the ratio of the accumulation area to the total glacier area: $AAR = Ac / Ts$ (where Ac is the accumulation area and Ts is the total surface). The AAR also remains stable, decreasing form 0,54 in YD to 0,51 in 2003. These values indicate that the glaciers on the SW slope of Nevado Hualcán have a very slight larger accumulation area.

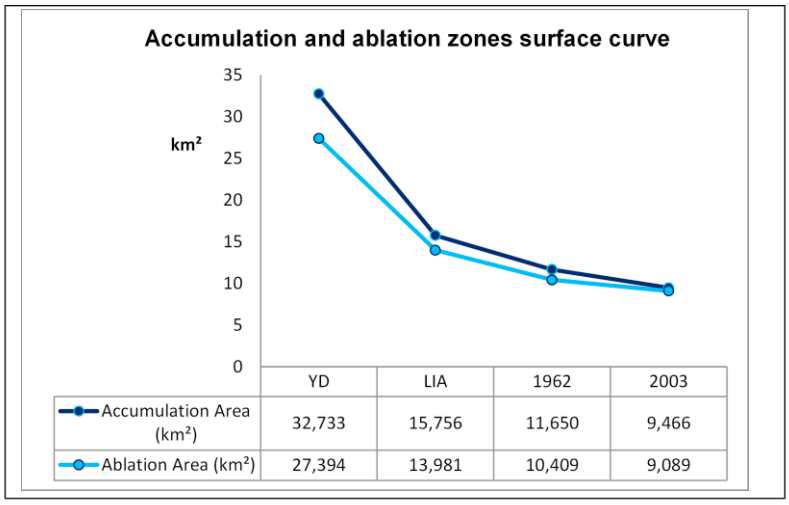

Figure 3. 11: Surface of the accumulation and ablation zones

Table 3. 7: Accumulation and ablation zones´ surfaces, their percentage respect to the total area of the glaciers, and AAR.

Glacial Phase	Accumulation Area (km²)	Ablation Area (km²)	Total Surface (km²)	% Accumulation	% Ablation	AAR
YD	32,733	27,394	60,127	54,44	45,56	0,54
LIA	15,756	13,981	29,737	52,99	47,01	0,53
1962	*11,650*	*10,409*	*22,059*	*52,81*	*47,19*	0,53
2003	9,466	9,089	18,555	51,01	48,99	0,51

Figures 3.12 and 3.13 show the mapping of Table 3.7 and Fig. 3.11. ELAs are mapped as the theoretical lines dividing the accumulation and the ablation zones, from which their respective surfaces were calculated. Whenever the ELA is above the upper limit of a glacier the accumulation zone disappears and the glacier is entirely in the ablation zone. In these conditions the mass balance of the entire glacier is negative, and thus it shall be condemned to disappear in the time needed for the environmental conditions to melt the remaining ice.

In summary, ELAs and their vertical shifts can be used to provide palaeoclimatic information. The simplest assumption it to attribute ELA changes entirely to temperature changes. However, changes in precipitation, humidity, radiation balance and wind speed have to be considered in order to achieve a reliable climatic interpretations.

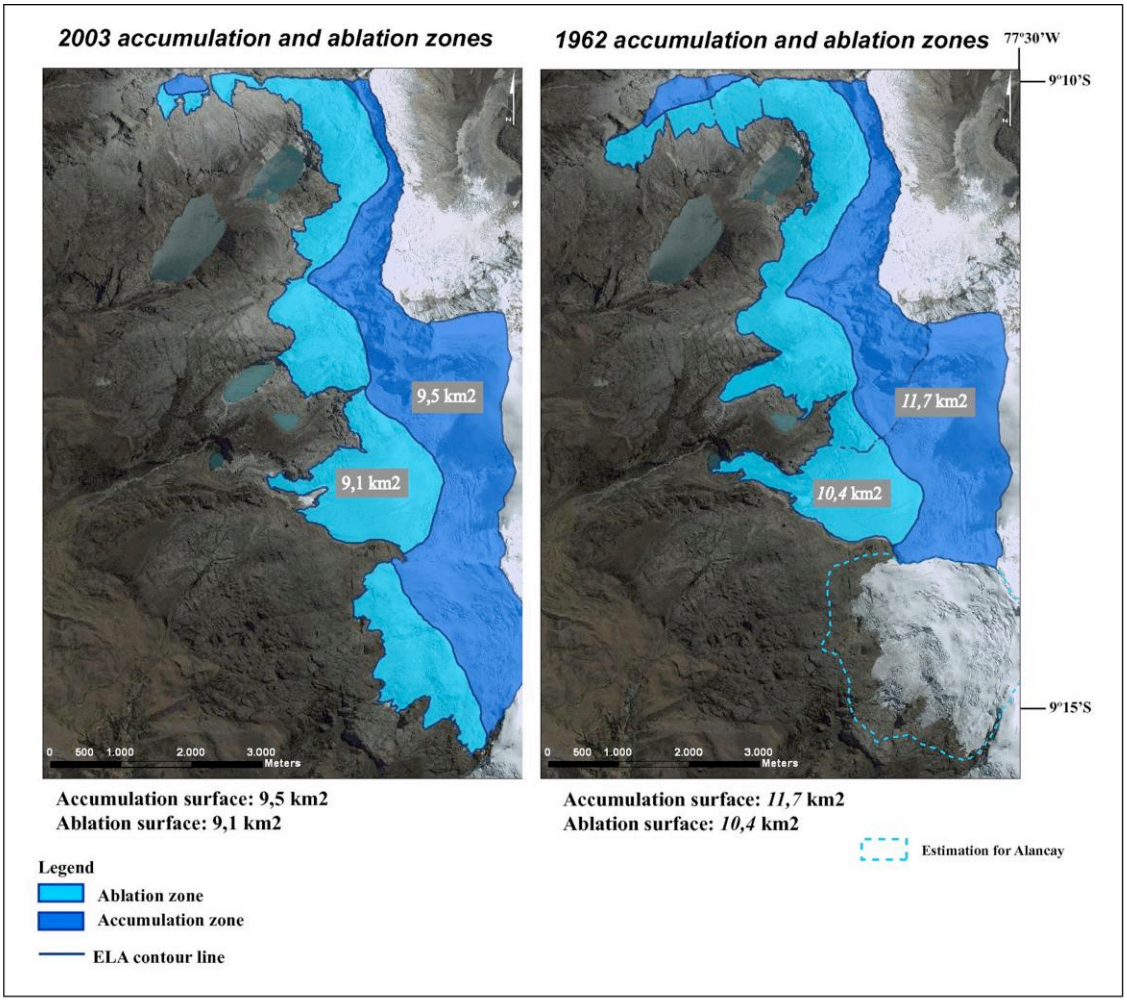

Figure 3. 12: Accumulation and ablation zones and their respective surfaces in 2003 and 1962.

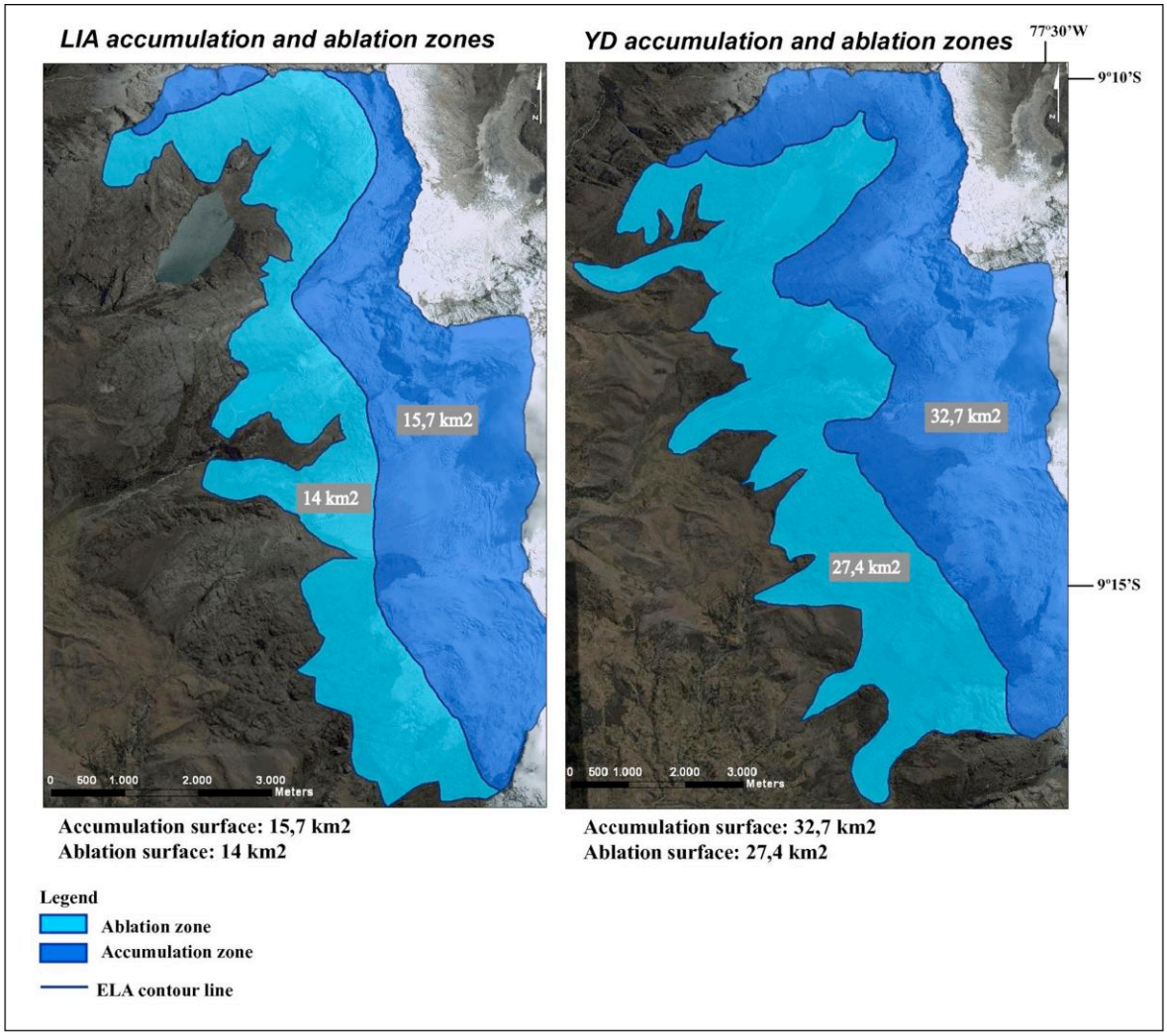

Figure 3. 13: Accumulation and ablation zones and their respective surfaces in LIA and YD.

CHAPTER 4

DISCUSSION AND FUTURE WORK

Tropical glaciers are highly expressive indicators of tropical climate, which is mainly characterized by homogeneous thermal conditions. As a result, the fluctuations of tropical glaciers can be directly traced to disturbances of simple climate parameters (Kaser, 1999). The aim of this work was to reconstruct earlier glacial phases in the SW slope of Nevado Hualcán in order to achieve quantitative information on surface areas and ELAs as a first step for further analysis on glacier evolution, glacier-climate relations and glacier hazards. The results of the present work show that: 1) the surface of glaciers has retreated 41,6 km² from YD to 2003 and 3,1 km² from 1962 to 2003, which corresponds to a deglaciation rate of 0,076 km²/year (76.000 m²/year). When compared to the deglaciation rate from LIA to 1962 (~0,025 km²/year), it shows that the rate of glacier retreat is increasing in recent times; 2) the ELA AABR vertical shift referred to 2003 was 472 m for YD, 130 m for LIA and 106 m for 1962, the latter corresponding to a vertical shift of 2,59 m/year; and 3) assuming that the changes in ELA correspond solely to changes in temperature, the estimated temperature shift from LIA to 2003 is of 0,78ºC.

4.1 Moraine mapping

The moraine mapping is important for paleo-glacier reconstruction because moraines are the geomorphological traces left by ancient glaciations. In the present work I used the 1962 aerial photographs and Google Earth to identify the moraines on the SW slope of Nevado Hualcán, and scientific publications to classify the moraines by their relative dating.

The results of this work show that moraines classified in Nevado Hualcán as preLLGM range from 3000 to 3500 m, LLGM moraines can be found between 3350 and 4080m, and postLLGM between 3460 and 4070 m. Farber et al. (2005) reported ^{10}BE exposure ages for 44 boulders moraines in four Cordillera Blanca Quebradas (Rurec, Cojup, Llaca and Queshque) and Smith et al. (2005) reported ^{10}BE cosmogenic ages from moraines in the eastern cordillera bordering Lake Junin. Both sets of results indicate that maximum ice volumes occurred during glacial periods before the LLGM sincethey find older moraines at altitudes below 3400 m. LLGM moraines in Quebrada Rurec (Farber et al. 2005) are found between 3400 and 3800 m, and moraines from the 20 to 16 ka BP still/readvances between 3800 and 4000m. In the present study, LLGM moraines in Nevado Hualcán were found at 200 m higher than in those studies, and the opposite happened to postLLGM moraines. This discrepancy may originate either from the different accuracy of relative dating methods as compared to direct methods, from differences in glacier behavior related to their locations and topography, or both. Smith et al. (2005) proposed that the

LLGM advance was caused by both an increase in precipitation and persistent cool temperatures.

For the YD glacial phase, the relative dating was based on Glasser et al. (2009). They proposed cosmogenic ^{10}BE dating of 21 moraine boulders in the Jeullesh and Tuco valleys using Lifton et al. (2005) scaling system. They reported three to four moraine building periods the biggest of which deposited large lateral moraines at 12,4/12,5 ka BP from 4290 m to 4411 m on the west slope of Jeullesh valley. Present data estimate the large YD lateral moraines from 3460 to 4480 m, 800 m below the moraines of Jeullesh valley. This difference in altitude may be explained by the altitude of the origins of the glaciers, which in Jeullesh is 5091 m and in Hualcán is 6125 m. However, this explanation is not compatible with data from the Huascarán-Chopicalqui massif where the different altitudes of glacier origins have almost no effect on the altitudes of their tongues which end at about the same elevation (Kaser 1995). Hence, the relative dating of the moraines classified as YD may need further study. The paleo-climatic records of Huascarán ice cores show a number of cooling events after 14,5 ka, which Glasser et al. (2009) prefer as a possible explanation for the YD glacier advances found at 12,5 ka BP.

Solomina et al. (2007) favor the use of lichenometry for dating in the high mountains of the Cordillera Blanca, at least for relative dating of deposits and landforms above the elevation of 3500 m. Their results on the moraines at glaciers in the Pacific facing slope suggest that peak LIA advance occurred between 1590 and 1720 and that the mean lichen sizes corresponding to this advance were from 29 to 30 mm. According to Thompson´s ice-core data from Huasacrán, these advances were triggered by both a decrease in temperature and an increase in snow accumulation. Future lichenometric studies in the SW slope of Nevado Hualcán may be useful to confirm the relative dating of the LIA moraines mapped in the present study to 4050 m and 4800 m.

In summary, the moraine mapping obtained in the present work based on relative dating chronologies shows that the altitudes of moraines here classified as LLGM and YD glacial phases differ from the ones reported in other publications by 200 and 800 m, respectively. This discrepancy may originate from the different methods used to calculate the chronology or from actual differences in glacier behavior in different areas. Further studies using absolute dating methods are required to clarify this issue.

4.2 Glacier delimitation and surface calculation

Glacier and paleo-glacier delimitation is important to achieve quantitative information on their areas and ELAs from which to reconstruct climate history. Here aerial photographs and Google Earth were used to delimit current glaciers, and moraine mapping to delimit paleo-glaciers.

The results obtained for single glaciers show that glacier Gatay2 in 2003 extended from above 5000 m to 4600 m and that of glacier Hualcán1 from 6000 m to 4300 m. The area of

glacier Hualcán1 was 11,4 km² in YD and 6,5 km² in 2003, and that of glacier Gatay2 was 6,9 km² and 2,1 km², respectively. Hastenrath et al. (1995) reconstructed the length, surface and volume changes of the SW facing glacier Yanamarey in southern Cordillera Blanca. They did so from historical data for six XXth centrury dates and from prominent moraines for an undated maximum extent. Glacier Yanamarey, as Gatay2, extended from above 5000 m to 4600 m in 1988. However, the area of Yanamarey was smaller than that of Gatay2 both in their maximum undated ice extent (1,7 km²) and in 1988 (0,8 km²). Nonetheless, the two glacier systems show a trend to decrease their surface areas, suggesting the presence of a general glacier retreat. Indeed, as shown in the results, the degalciation rate from 1962 to 2003 was 0,076 km²/year, and that estimated from the period between the LIA period and 1962 was 0,025 km²/year, indicating that the rate if glacier retreat has actually accelerated during the XXth century.

One other area reconstruction of the Cordillera Blanca has been done by Silverio et al (2005). They used Landsat TM images of 1987 and 1996 to map the glaciated area of the entire Cordillera Blanca, and used the NDSI (Normalized Difference Snow Index) on the satellite images to differentiate glaciers from the surrounding moraines. This index does not discern snow from glacial ice and, therefore, the results may overestimate the real ice surface. The values obtained by these authors for glacierized areas were 643±63 km² in 1987 and 600±61 km² in 1996. These results were compared to an estimate of 721 km² in 1970 obtained by Hidrandina (see table 1.2) for the “Inventario de glaciares de Perú”. They suggested that the area of glaciers had retreated more than 15% in 25 years, with a surface retreat rate of 4,8 km²/year from 1987 to 1996 (9 year period). The data on Nevado Hulcán obtained in the present work do not match completely with the above observations. On Nevado Hualcán, the total surface of glaciers was 18,55 km² in 2003, and of 22,06 km² in 1962, corresponding to a surface retreat of 15,9% in 41 years, and a retreat rate of 0,076 km²/year, much lower than the estimation done by Silverio et al (2005). One possible explanation of this discrepancy is that Silverio´s work covered the entire Cordillera Blanca, whereas the present study focused on one single valley, impeding a direct comparison. Another explanation can be found in the different methods used to calculate glacier surface areas. Silverio used automatic NDSI classification method on satellite images to differentiate the glacier from the surrounding moraines, but this does not discern snow from glacial ice. In the present study, photointerpretation methods allowed differentiating snow from glacial ice, as described in part 2.4, and this provides more accuracy to glacier delimitation.

Glacier areas and retreat rates for the glaciers in Volcán Nevado Coropuna massif have been previously repoted by Silverio (2004) and Úbeda (2010). The former used the method described above, and the latter the ones used in the present work and detailed in part 2.4. The deglaciation rates obtained by Silverio (2004) were higher than the ones in Úbeda (2010), in some cases they differed by more than 2 km²/year. As commented above, this difference is probably related to the method used to delimit glaciers. The mean deglaciation rates reported by Úbeda for the SE sector of Nevado Coropuna for the 41 year period from 1986 to 2007 was found to be very similar to the ones on the SW slope of Nevado Hualcán in the 41 period from 1962 to 2003 reported here. Úbeda obtains a

deglaciation rate of 0,0078 km²/year for the SE sector and the present work records a 0,076 km²/year. Given that the delimitation methods employed in both cases were the same, this suggests that the two geographical domains behave similarly with respect to the speed of glacier retreat, even being separated by 6º latitude and not sharing similar climatic conditions.

The delimitation and surface calculation of tropical glaciers offer important quantitative information on glacier evolution. Nevertheless, only the changes in volume, which represent the changes in mass, can be converted into energy equivalents. Thus, it is important to model the ice volume of the former and current glaciers. Future research will require direct glaciological methods such as mass balance measurements and climatic measurements of air and soil temperature and precipitation in order to study both the climate change in current glaciers and the paleo-climatic conditions of former glaciers.

4.3 ELAs AABR

Changes in ELA provide paleo-climatic information because they depend on an interaction of climatic processes associated with accumulation and ablation on glaciers. Paleo-climatic interpretations have to face difficulties in separating the effects of temperature, precipitation and radiation changes, but still represent one of the few methods available for investigating paleo-climate in central Andes (Klein et al. 1999).

In the present study I calculated ELAs for the SW slope of Nevado Hualcán following the AABR method (Area x Altitude Balance Ratio). The results show ELA AABR altitudes of 4652 m for YD, 4994 m for LIA, 5018 m for 1962 and 5124 m for 2003. The corresponding altitude shifts, with respect to 2003, were 472 m from YD, 130 m from LIA and 106 m from 1962, the latter corresponding to a vertical shift of 2,59 m/year.

There are several methods to calculate current and former ELAs but their detailed analysis exceeds the purpose of this work. I shall discuss few of them in relation to the data reported here for Nevado Hualcán.. The results for Nevado Hualcán compare well with the data obtained in Volcán Nevado Coropuna (15ºS,72ºW) by Úbeda (2010). This author found that the altitude of ELA AABR in the SE sector was 5776 m for LIA, and 5844 m for 2007, reporting a vertical shift of 2,19 m/year from 1986 to 2007. The results in the present work suggest an ELA AABR altitude of 4994 m in LIA, of 5124 m in 2003 and a shift of 2,59 m/year from 1962 to 2003. The altitudes of ELAs in Hualcán are lower than those in Coropuna by 782 m in LIA and 712 m in 2007, suggesting differences in climatic and paleo-climatic conditions between these two domains. These two regions are located at 15ºS 72ºW (Coropuna) to 9ºS 77ºW (Hualcán). Further studies on climatic and paleo-climatic differences between Cordillera Blanca and Volcán Nevado Coropuna massif will support this possibility.

Different AAR values (Accumulation Area Ratio) for tropical glaciers have been published and the selection of one or another leads to different altitudes of ELA AAR. This raises the

question of what is the value to be used in Nevado Hualcán. ELAs AAR for the East to West Pucajirca-Santa Cruz transect were calculated for 1930 and 1950 by Kaser and Georges (1997). They assumed a mean value of AAR = 0.75 for the Cordillera Blanca. However, Kaser and Osmaston (2002) considered the value AAR=0,67 as the most appropriate for tropical glaciers, and Úbeda (2010) obtained a mean value of AAR=0,58 for glaciers in Volcán Nevado Coropuna. In the present study, the values of AAR for the SW slope of Nevado Hualcán were found to range from 0,54 in YD to 0,51 in 2003, which are very close to those of Úbeda (2010). This is probably related to the similarity in the methods used to delimit glaciers. However, further work is required to compare different ELA methods in order both to validate the ELA results here presented and to estimate the most adequate AAR value for the Cordillera Blanca.

The data of ELAs AABR reported here fit well also with those obtained by other different methods. Klein et al. (1999) adopted the “snowline”, i.e. the lower limit of perennial snow cover or glaciers, as an approximation of the 1962-63 ELA, assuming that the altitude trend goes in parallel for both. For LLGM glaciers, they calculated the ELA by the THAR method (Terminus-to-Headwall Altitude Ratio). Klein´s study was aimed at a regional scale in Central Andes, hence, their results at smaller scales may carry significant errors. They determined a modern snowline for central Perú at 5100 m, which is consistent with the result obtained in the present work for the ELA AABR in 2003 at 5124 m. ELA AAR values of the W facing slopes of Santa Cruz, Alpamayo and Pucajirca for 1950, were reported at 5068, 5019, and 4958 m respectively (Kaser and Georges, 2007). These values are very similar to the ELA AABR value obtained in the present study, which for 1962 was 5018 m.

Asymmetries in ELAs from East to West and from East facing to West facing slopes were observed by Kaser and Georges (1997), which arises the question of whether these asymmetries can also be found in the Nevado Hualcán. Kaser and Georges (1997) found two contradictory asymmetries: ELAs are lower from East to West throughout the general transect, but the opposite asymmetry is found within Santa Cruz and Alpamayo massifs, which have lower ELAs AAR on their West facing slopes. They suggest several possible causes related to the particularities of atmospheric circulation in the tropics related to convective activity decreasing to the west and to the diurnal convective circulation system (see part 1.3). Following their suggestions, a similar study may be completed to the entire Hualcán Massif from Nevado Ulta to Nevado Copa so as to determine two possible behaviors of ELA spatial variation: the asymmetry between SW and NE slopes, and the asymmetry between Northern and Southern locations.

From ELA values, it is possible to estimate climatic changes. The simplest climatic interpretation of ELA assumes that the changes in ELA (ΔELA) are entirely a function of the changes in temperature (ΔT), which can be estimated by using a selected MALR. A key point in the estimation of temperature changes is the selection of the value of MALR. In the present study, the MALR value used was 6ºC/km (Rex 1969; Klein et al. 1999, discussed in Úbeda, 2010). This gave a temperature shift of 0,78ºC from LIA to present, suggesting a substantial increase in temperature for the period. However, Úbeda (2010) calculated the specific MALR of Nevado Coropuna by direct climatic measurements of

8,4ºC/km. From this value, he inferred a temperature shift of 0,7ºC from LIA to present. Therefore, the values for Nevado Hualcán fit well with Nevado Coropuna in spite of the differences in MALR. Such a coincidence may originate from actual differences in the value of MALR between Nevado Hualcán and Coropuna, but one other possibility is an inaccurate estimation of temperature changes for the Nevado Hualcán. This highlights the importance of having specific MALR of Nevado Hualcán by direct climatic measurements.

Direct climatic measurements would also allow mapping the 0ºC isotherm in order to compare it to the ELA altitude. Klein et al. (1999) pointed that ELA in the tropics is strongly dependent to the position of the 0ºC isotherm because the lack of thermal seasonality leads to a relatively constant altitude of the 0ºC isotherm throughout the year. Thus, an ELA lying at or below the level of the 0ºC isotherm is primarily sensitive to temperature changes whereas an ELA lying above the level of the 0ºC isotherm is much more sensitive to accumulation changes (Klein et al., 1999).

4.5 Conclusions

"Glaciers and ice caps constitute *Essential Climate Variables* (ECV) within the *Global Climate Observing System* (GCOS) and its terrestrial component, the *Global Terrestrial Observing System* (GTOS), as related to the *United Nations Framework Convention on Climate Change* (UNFCCC)" (WGMS, 2008).

Glaciers are not only key indicators of global climate change, but also a water supply upon which depend an increasing amount of people, and a source of natural hazards. By the study and monitoring of glaciers, the rate of change can be quantified, climatic interpretations may be inferred, and future climate change scenarios predicted. In this way, the processes of climate change adaptation and disaster risk reduction can be assessed and advised.

This project was triggered by the GLOF form Lake 513 which took place the 11th of April 2010 in the SW slope of Nevado Hualcán. The aim of this work was to reconstruct earlier glacial phases in the SW slope of Nevado Hualcán in order to generate quantitative information on surface areas and ELAs as a first step for further analysis on glacier evolution, glacier-climate relations, glacier hazards and climate change.

The specific conclusions of the present report are:

1) Moraines on the SW slope of Nevado Hualcán were identified and mapped and served as the reference to reconstruct the geometry of paleo-glaciers in the LIA and YD glacial phases. Current glaciers were also delimited for 1962 and 2003 using aerial photographs and Google Earth.
2) From the delimitation of glaciers, their correspondent surface areas were calculated and compared. The results show that the surface of glaciers has retreated 41,6 km² from YD to 2003 and 3,1 km² from 1962 to 2003, which corresponds to a deglaciation

rate of 0,076 km²/year (76.000 m²/year). The results match with the general decreasing trend previously observed by other authors.

3) From the delimitation of glaciers, their ELAs AABR were calculated. The results show an altitudinal shift of the ELAs AABR from YD to 2003: the vertical shift respect to 2003 was 472 m from YD, 130 m from LIA and 106 m from 1962, this last corresponds to a vertical shift of 2,59 m/year. When the ELA altitude shifts above the upper limit of a glacier, its accumulation zone disappears, and also its positive mass balance, thus the glacier will be condemned to disappear. The results show that ELAs in the SW slope of Nevado Hualcán are in some cases just 162 m below the upper limits of glaciers, revealing prompt terminal stages of some glaciers.
4) Changes in ELAs are caused by changes in climatic conditions. As a first approximation, it was assumed that the changes in ELA corresponded solely to changes in temperature. The temperature shift from LIA to 2003 was estimated to be 0,78ºC.

REFERENCES

Ames, A. and Francou, B. (1995). Cordillera Blanca. Glaciares en la Historia. Bulletin de l´ Institute Frrançais d´ Etudes Andines, 24(1), 37 – 64.

Andrés, N. (2009). Técnicas de Información Geográfica aplicadas al studio del origen de los lahares y su experimentación en estratovolcanes tropicales. Universidad Complutense de Madrid.

Benn, D. I., Owen, L. A., Osmaston, H. A., Seltzer, G. O., Porterd, S. C. and Mark, B. (2005). Reconstruction of equilibrium-line altitudes for tropical and sub-tropical glaciers. Quaternary International 138–139, 8–21.

Carey, M. (2010). In the shadow of melting glaciers. Climate change and Andean society. Oxford University Press.

Carey, M., Huggel, C., Bury, J., Portocarrero, C. and Haeberli, W. (2010). An Integrated Socio-Environmental Framework for Climate Change Adaptation and Glacier Hazard Management: Lessons from Lake 513, Cordillera Blanca, Peru. Manuscript in preparation.

Farber, D. L., Hancock, G. S., Finkel, R. C. and Rodbell, D. T. (2005). The age and extent of tropical alpine glaciation in the Cordillera Blanca, Peru. Journal of Quaternary Sciences, 20, 759–776.

Garver, J.I., Reiners, P.W., Walker, L.J., Ramage, J.M. and Perry, S.E. (2005). Implications for Timing of Andean Uplift from Thermal Resetting of Radiation-Damaged Zircon in the Cordillera Huayhuash, Northern Peru. The Journal of Geology, 113, 117–138.

Georges, C. (2004). 20th-Century Glacier Fluctuations in the Tropical Cordillera Blanca, Peru. Arctic, Antarctic, and Alpine Research 36, 100-107.

Glasser, N. F., Clemmens, S., Schnabel, C., Fenton, C. R. and McHargue, L. (2009). Tropical glacier fluctuations in the Cordillera Blanca, Peru between 12.5 and 7.6 ka from cosmogenic 10Be dating. Quaternary Science Reviews, 28, 3448–3458.

Gregory-Wodzicki, K.M. (2000). Uplift history of the Central and Northern Andes: A review. GSA Bulletin, 112, 7, 1091–1105.

Hastenrath, S. and Ames, A. (1995). Recession of Yanamarey Glacier in Cordillera Blanca, Peru, during the 20th century. Journal of Glaciology 41 (137), 191–196.

Huggel, C., Haeberli, W., Kääb, A., Bieri, D. and Richardson, S: (2004). An assessment procedure for glacial hazards in the Swiss Alps. Canadian Geotechnical Journal, 41, 1068-1083.

Habereli, W. (2010): Glaciers in an environmental context Part 1: Paleoglaciology. Department of Geography, University of Zurich

Kääb, a., Huggel, C., Barbero, G., Chiarle, M., Cordola, M., Epifani, F., Haeberli, W., Mortara, G., Semino, P., Tamburini, A. and Viazzo, G. (2004). Glacier hazards at Belvedere glacier and the Monte Rosa East face, Italian Alps: processes and mitigation. Internationales Symposion, Interpraevent, Riva / Trient.

Kaser. G. (1999). A review of the modern fluctuations of tropical glaciers. Global and Planetary Change 22, 93–103.

Kaser, G. (1995). Some notes on the behavior of tropical glaciers. Bulletin de l´ Institute Frrançais d´ Etudes Andines, 24 (3), 671-681.

Kaser, G., Ames, A. and Zamora, M. (1990). Glacier fluctuations and climate in the Cordillera Blanca, Perú. Annals of Glaciology, 14, 136 – 140.

Kaser, G., Fountain, A. and Jansson, P. (2003). A manual for monitoring the mass balance of mountain glaciers. UNESCO, International Hydrological Programme.

Kaser, G., Georges, C. (1996). On the mass balance of low latitude glaciers with particular consideration of the peruvian Cordillera Banca. Geografiska Annaler, 81A, 643 – 651.

Kaser, G. and Georges, C. (1997). Changes of the equilibrium line altitude in the tropical Cordillera Blanca (Perú) between 1930 and 1950 and their spatial variations. Annals of Glaciology 24, 344-349.

Kaser, G., Juen, I., Georges, C., Gómez, J. and Tamayo, W. (2003). The impact of glaciers on the runoff and the reconstruction of mass balance history from hydrological data in the tropical Cordillera Blanca, Peru. Journal of Hydrology 282, 130–144.

Klein, A.G., Seltzer, G.O. and Isacks, B.L. (1999). Modern and last local glacial maximum snowlines in the Central Andes of Peru, Bolivia, and Northern Chile. Quaternary Science Reviews, 18, 63-84.

McNulty, B. and Farber, D. (2002). Active detachment faulting above the Peruvian flat slab. Geology, 30, 6, 567–570.

Nussbaumer, S.U. (2010). Continentalscale glacier variations in Europe (Alps, Scandinavia) and their connection to climate over the last centuries. Inauguraldissertation der Philosophisch-naturwissenschaftlichen Fakultät der Universität Bern.

Osmaston, H.A. (2005). Estimates of glacier equilibrium line altitudes by the AreaxAltitude, the AreaxAltitude Balance Ratio and the AreaxAltitude Balance Index methods and their validation. Quaternary International, 138–139, 22–31.

Silverio, W. and Jaquet, J-M. (2005). Glacial cover mapping (1987–1996) of the Cordillera Blanca (Peru) using satellite imagery. Remote Sensing of Environment, 95, 342–350.

Smith, J.A., Seltzer, G.O., Farber, D.L., Rodbell, D.T. and Finkel, R.C. (2005). Early Local Last Glacial Maximum in the Tropical Andes. Science, 308, 5722, 678-681.

Smith, J.A., Mark, B.G., and Rodbell, D.T. (2008). The timing and magnitude of mountain glaciation in the tropical Andes. Journal of Quaternary Science, 23(6-7), 609–634.

Solomina, O., Jomelli, V., Kaser, G., Ames, A., Berger, B. and Pouyaud, B. (2007). Lichenometry in the Cordillera Blanca, Peru: “Little Ice Age” moraine chronology. Global and Planetary Change 59 225–235.

Thompson, L G, Mosley-Thompson, E., Davis, M. E., Lin, P-N, Henderson, K.A., Cole-Dai, J., Bolzan, J.F. and Liu, K.B. (1995). Late glacial stage and Holocene tropical ice core records from Huascaran, Peru. Science, 269, 5220, 46-50.

Úbeda, J. (2010). El impacto del cambio climático en los glaciares del complejo volcánico Nevado Coropuna (Cordillera Occidental de los Andes Centrales). Universidad Complutense de Madrid,.

WGMS (2008). Global glacier changes: facts and figures. UNEP-WGMS.

ACKNOWLEDGEMENTS

I´d like to thank David Palacios and Wilfried Haeberli for suggesting me this project and for the help with the research. I would also like to thank the coordinator and the teachers of the Master in TIG, the Geography degree and the members of the GFAM. My deep thanks to José Úbeda for his enthusiasm and generous help. Also my gratitude to Sres. Lionel Fidel Smol and Patricio Valderrama (INGEMMET) for providing the SPOT image and the DEM; and Sr. Marino Zamora for sending the aerial photographs from IGN-Perú to Madrid. Finally, a special thanks to my parents and my sister Julieta for their unconditional support.